UNIVERSITY OF OKLAHOMA

GRADUATE COLLEGE

A SYSTEMATIC APPROACH FOR UPSCALING OF THE EOR RESULTS FROM LAB-SCALE TO WELL-SCALE IN LIQUID-RICH SHALE PLAYS

A THESIS

SUBMITTED TO THE GRADUATE FACULTY

in partial fulfillment of the requirements for the

Degree of

MASTER OF SCIENCE

By

EMMANUEL AKITA
Norman, Oklahoma
2020

A SYSTEMATIC APPROACH FOR UPSCALING OF THE EOR RESULTS

FROM LAB-SCALE TO WELL-SCALE IN LIQUID-RICH SHALE PLAYS

A THESIS APPROVED FOR THE
MEWBOURNE SCHOOL OF PETROLEUM AND GEOLOGICAL ENGINEERING

BY THE COMMITTEE CONSISTING OF

Dr. Rouzbeh Moghanloo, Chair

Dr. Ali Tinni

Dr. Omidreza Mohammadzadeh

To my caring parents, Rebecca and Theophilus, and my siblings, Princess Daisy and Paul.

Thanks for all the love, encouragement, and support.

Abstract

Breakthrough technologies such as horizontal drilling and hydraulic fracturing have led to game-changing results in the oil and gas industry. With the increase in energy demand and the overall growth in oil production in the United States, unconventional resources have become extremely attractive to exploit this end. The breakthrough technologies help make possible the exploitation of resources from tight plays since their characteristic low permeability and low porosity have made them previously uneconomic. Well stimulation and completion technologies have been researched and improved over the past few decades as scientists and engineers aim to increase the production of hydrocarbons from hydraulically fractured wells.

This thesis explores equations to describe recovery factors of EOR processes in oil shale plays. The existing studies imply promising future for implementing gas cyclic injection through hydraulically fractured wells completed in shale plays; the EOR agent (a mixture of HC gas or CO2) is injected and after a soaking period, the well is put back on production. However, translation of lab-scale EOR results to field-scale is yet to be resolved. Dynamic penetration volume (DPV) controls the amount of contacted oil by the EOR agent (fluid-fluid interface) and slowly grows with the square root of time, and limits the recovery efficiency in the pilot-scale. The main idea proposed in this thesis is developing a systematic approach to

upscaling the EOR recovery in lab-scale to field-scale. Modeling and experimental methods are used to investigate potential recovery loss in well-scale compared to recovery measured in the lab-scale. In this formulation, the recovery in pilot-scale is defined as the product of recovery in lab-scale and field factor. Recovery in lab-scale is a function of pressure drawdown during production (choke effect). Choke-size controls how fast the mixture of gas and vaporized oil components will be produced back after soaking time.

The field factor entails two parameters that control how much of in-situ liquid hydrocarbon can potentially interact with EOR agent. It is evaluated as the fraction of reservoir volume prescribed within inter-well spacing accessible to the EOR agent when injection process begins. The pore connectivity loss can occur because of the physical closure of flow path at the fracture-matrix interface and/or two-phase blockage. The limiting two phase phenomena can potentially prevent the injected gas from getting into pore space because of capillary forces.

The results suggest that recovery in the pilot-scale can be significantly reduced owing to pore connectivity loss (a factor of two). The pore connectivity is reduced as pore pressure decreases and effective stress increases. Change of fluid conductivity is evaluated under stress and differentiate contribution of pore connectivity loss and pore shrinkage. Also, the concept of Biot number is

introduced, which lumps together all parameters unaccounted for on the field scale, and thus helps to use similar equations at different scales, providing a systematic approach. Moreover, the results suggest that chokes size effect observed in the experiments can be explained by loss of pore connectivity. Finally, field factor values are calculated and determined as being between 0 and 1.

Acknowledgments

I would like to express my sincere gratitude to Dr. Rouzbeh Moghanloo for his continuous academic support and encouragement. His immense knowledge and insight have greatly helped in designing the model for this EOR work. I felt humbled to have been given the opportunity to work with him in my master's career. Dr. Moghanloo was very understanding and always motivating, trusting the decisions I made and advised me along the way. He also pushed me to realize my true potential.

I would also like to thank Dr. Ali Tinni for his critical suggestions and contributions to this work in the form of experimental tests. His phenomenal insight in petrophysics helped greatly in crafting this research study. I am very grateful to him for taking an interest in my research and providing valuable recommendations.

Furthermore, I am thankful to Dr. Davud Davudov for always being there when I needed him. His expertise in modeling helped immensely in putting together this research. Finally, I would like to thank Dr. Mohammadzadeh for showing interest in my work, and for his continued support during this period.

Table of Contents

List of Tables

List of Figures

Chapter 1. Introduction

1.1 Overview

Breakthrough technologies such as horizontal drilling and hydraulic fracturing have led to game-changing results in the oil and gas industry. With the increase in energy demand and the overall growth in oil production in the United States, unconventional resources have become extremely attractive to exploit this end. The breakthrough technologies help makes possible the exploitation of resources from tight plays since their characteristic low permeability and low porosity have made them previously uneconomic. Well stimulation and completion technologies have been researched and improved over the past few decades as scientists and engineers aim to increase the production of hydrocarbons from hydraulically fractured wells (**Figure 1,** EIA, 2016)

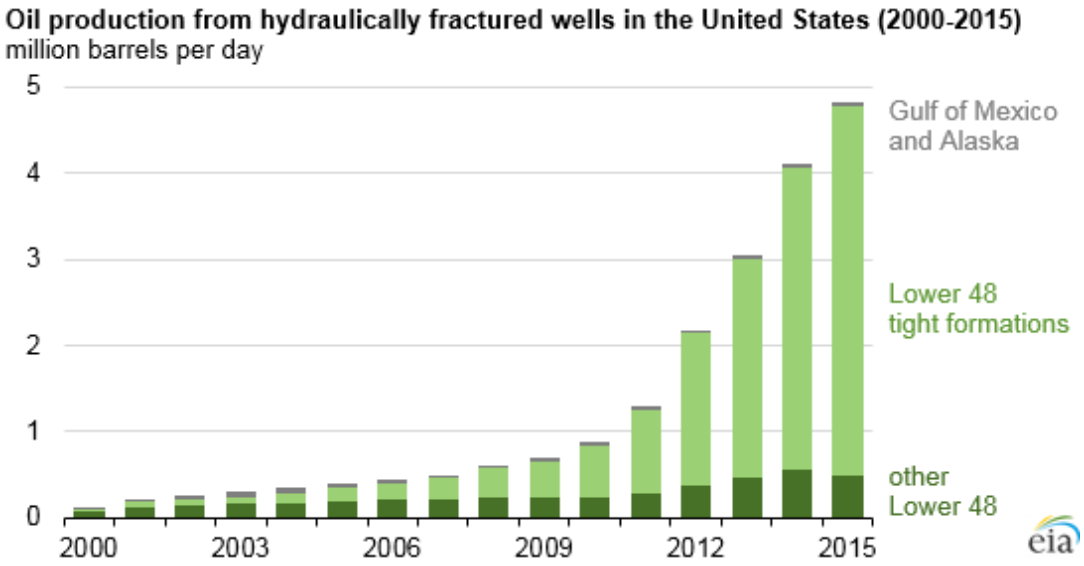

Figure 1. Oil production from hydraulically fractured wells in the US (EIA, 2016)

Yu and Sheng (2015) presented simulation model results and saturated core studies which highlight the fact that the "huff-n-puff" technique could be used to recover more than 50% oil in place. Following the change of the U. S's oil Market from a net importer to a net exporter, imported oil consumption has never been lower in the United States, dropping to 11% (EIA, 2016). There is an estimated 900 billion barrels of original oil in place of recoverable oil in Bakken only (Alfarge et al., 2017). As a world-leading crude producer, there is an urgent need to address the low recovery factor from tight formations, which is on average, less than 10% (Hoffman and Evan, 2016). Furthermore, this urgent need to exploit tight formations has been underscored by increased development in unconventional

liquid-rich plays in the Bone Springs, Eagle ford, Bakken and Wolfcamp (EIA, 2016).

From current research, cyclic gas injection in hydraulically fractured wells have shown promising results, which could improve the recovery factors in the future. However, laboratory results are not necessarily consistent with field results, and this issue is yet to be solved. This owes to the myriad unaccounted variables in the field tests, which are difficult to simulate in the lab. The amount of oil contacted by Huff and Puff gas injection EOR is controlled by the so-called dynamic penetration volume (DPV). DPV is directly proportional to $\sqrt{time}$, due to the growth of mixing zone in dispersive flow, Lake, 1989, Moghanloo, 2012, Shen et al., 2017). It significantly affects the recovery efficiency in the field. This research project aims to propose a systematic method to be used to upscale the EOR recovery in lab-scale to field-scale.

The upscaling process is achieved through modeling, and experimental investigative work. These techniques allow to determine the possible loss in recovery when translating EOR lab results to the field. Here, lab-scale recovery is multiplied by a field factor to get the additional added recovery in the field scale due to EOR. As discussed later on, lab-scale recovery is a function of pressure drawdown during production due to the choke effect. Thus, the speed at which gas and vaporized oil components will be produced back after soaking time is controlled by choke-size.

Field factor in this work is analyzed as the fraction of the reservoir volume which is accessible to the EOR agent at the beginning of injection. It essentially helps to determine the added hydrocarbon recovery from a field-scale project, based on lab-scale recovery results. It consists of two parameters that control the amount of liquid hydrocarbons in the formation that could possibly interact with an EOR agent. It is determined by multiplying the fraction of reservoir volume stimulated during fracturing by the stimulated reservoir volume fraction (SRV) accessible to EOR agent (DPV/SRV) at any given time. The governing parameter of SRV is the fracture treatment efficiency. There can be loss of pore connectivity, which arises due to the closure of the fracture-matrix interface flow path and/or two-phase blockage. The limiting two phase phenomena can potentially prevent the injected gas from getting into pore space because of capillary forces.

The increase in effective stress and decrease in pore pressure leads to reduction in pore connectivity. As will be later seen, pore connectivity can significantly reduce the field-scale results (a factor of two), as suggested from results in this work. The change of fluid conductivity under stress is evaluated, and the contribution of pore connectivity loss and pore shrinkage is differentiated. Moreover, Biot number is a new concept introduced in this line of research. This lumps together all parameters unaccounted for on the field scale. This use of the Biot number allows for similar equations at different scales, thus providing a systematic approach. Furthermore, the results of this work suggest that pore connectivity loss could explain choke size

effect which is observed in experimental work. Finally, it is also observed that total recovery is a function of the diffusivity coefficient. This seems to not be significantly changed by different ratios of fracture to matrix volumes.

This work presents a novel approach to upscale the EOR results obtained in lab-scale to field-scale. The outcome is expected to help operators with the pilot-test performance evaluations.

1.2 Motivation

Researchers report that the primary oil recovery in unconventional shale plays is typically less than 10% (Wan and Sheng, 2015, Yuan et al., 2017). To economically exploit hydrocarbon resources from unconventional formations, the use of EOR techniques is a must. It has been indicated that there is a big gap between lab-scale recoveries and pilot-test performance (Alfarge et al., 2017). It's been argued that this gap is typically due to injection induced fractures (IIF) that promote inter-well connectivity issue and reduce the interaction surface between EOR agent and the resident oil (Alfarge et al., 2017).

The difference in conventional and unconventional EOR applications are looked at from two dimensions as stated below:

1. The EOR agent – oil interaction at the interface is limited in unconventional shale plays compared to conventional reservoirs. This is due to the presence

of micro fractures in the system and loss of pore connectivity. So even though there exists large fractures within the system, there are micro fractures also which limit the penetration length When injected into the formation, the fluid would flow through a fracture network (consists of created and connected natural fractures) and diffuse into shale matrix. This then allows for fluid-fluid interaction at the fracture-matrix interface, as the fluid contacts the oil molecules. A limiting factor for ultimate recovery is the fracture network considered, which will be a percentage of inter-well spacing during fracturing treatment.

Due to low pore connectivity in shale matrix, counter-current diffusion of gas molecules and co-current diffusion out of the matrix are very slow processes. Counter-current diffusion has been observed in our lab experiments, and is the movement of gas molecules into the matrix (during the injection and soaking time). Whereas co-current diffusion refers to the movement of the matrix (during production stage). These processes control the evolution of the EOR agent fluid-hydrocarbon interface. The counter-current diffusion occurs during the injection and soaking time, while the co-current diffusion occurs during production time, and they are very slow processes. Following Moghanloo (2013 and 2014)

$$\frac{\text{Scaling factor}_{\text{pilot-scale}}}{\text{Scaling factor}_{\text{lab-scale}}} = \frac{D_{pilot\text{-}scale}}{D_{lab\text{-}scale}} \times \left(\frac{L_{lab\text{-}scale}}{L_{pilot\text{-}scale}} \right)^2 \quad (1)$$

Where $D_{\text{pilot-scale}}$ and $D_{\text{lab-scale correspond}}$ to the diffusion rate, in ft. /sec^2 in the field and the lab respectively, and $L_{\text{lab-scale}}$ and $L_{\text{pilot-scale}}$ correspond to the half fracture spacing in ft. in the lab and the field respectively.

Hence, unless massive micro fractures created during pilot test near shale matrix-fracture interface, the scaling factor for diffusion transport process in field-scale will be very small compared to that of lab-scale; in other words, the recovery factor of a pilot-test would be significantly smaller for the same dimensionless time.

2. Due to pressure drop during production phase after injections stops, there is loss of pore connectivity. It is postulated that this choke effects which is observed in the lab experiments is due to connectivity loss at the matrix-fracture interface.

Dynamic penetration volume (DPV) for injected EOR agent is defined very similar to the notion of dynamic drainage volume (DDV) which occurs when there is propagation of pressure disturbance created at the production well throughout the reservoir. This is different from the fixed-boundary, boundary-dominated flow, as this is a moving-boundary problem. Here, the size of DPV grows with$\sqrt{time}$.

This leads to the proposed equation below for upscaling lab-scale results to field scale. $\frac{DPV}{SRV}$ slowly increases with $\sqrt{time}$ (growth of mixing zone in dispersive flow,

Lake [1989], Moghanloo [2012], Shen et al. [2017]). Also, SRV has been shown to be only a fraction of inter-well spacing (Yuan et al., 2017). Thus, field factor is always between 0-1 and always reduces the expected recovery factors in the field-scale.

$$\text{Recovery}_{\text{Pilot-scale}} = \text{Recovery}_{\text{Lab-scale}} \times \underbrace{\text{Field Factor}}_{\left(\frac{DPV}{SRV}\right)\times\left(\frac{\text{SRV}}{\text{Inter-well spacing}}\right)} \tag{2}$$

A penetration distance is defined as penetration length, L_p, as the injected gas only penetrates some portion of the matrix. Also, the accessibility (field) factor is defined as

$$\frac{DPV}{Inter-well\ spacing} = \frac{Lp}{L} \tag{3}$$

Where DPV is the dynamic penetration volume, L_p is the distance of matrix penetrated by the gas, and L is the half length of the system.

Eq. 3, allows to apply lab results to the field scale. The discrepancy between lab-scale and field-scale tests could be argued as arising from ignoring the field factor, as seen in **Eq. 2**. Yuan et al. (2017) showed how small the field factor could be (0.1).

1.3 Synopsis

This thesis is structured in 5 chapters:

Chapter 1 provides a brief introduction and background to Unconventional Resources and the need for Enhanced Oil Recovery. Chapter 2 provides a literature review that details different types of EOR techniques available, their efficacy and the previous lab and modeling work done. Chapter 3 describes the methodology used in this work, both experimental and modeling. Here, a mathematical modeling of huff-n-puff process is first presented; next, our experimental work on the choking effect in an EOR test is presented; next, we try to theoretically explain why this so-called choke effect could occur. Chapter 4 lists the results and interpretation of the findings. This involves a sensitivity analysis of different parameters involved in the Huff-n-Puff process. Chapter 5 lists the major findings of this research and their contributions towards improving the state of EOR in Unconventional Resource Development, the limitations of this research study and future work.

Chapter 2. Literature Review

2.1 EOR Economics and Pilot Tests

Since shale production is highly economical, it is extremely necessary to utilize EOR in stimulating hydrocarbon production from unconventional reservoirs. More importantly, it is essential to optimize every step of the stimulation process including the selection of reservoir candidates, suitable EOR methods, and the optimal operational implementation for the selected methods. However, there are undoubtedly financial challenges with long-term EOR investments, including injection gas, production loss during choking time, and cost of compressors. **Table 1** shows some of the EOR pilot tests conducted

Table 1. Modified summary of EOR pilot tests with different techniques (Wang et al., 2017)

No	Operator	Formation	State	Year	Fluid	Type
1	EOG	Bakken	ND, US	2008	CO_2	Huff-n-puff
2	–	Bakken	MT, US	2009	CO_2	Huff-n-puff
3	EOG	Bakken	ND, US	2012	Water	Huff-n-puff
4	EOG	Bakken	ND, US	2012–2013	Water	Flooding
5	EOG	Bakken	ND, US	2014	Natural gas	Flooding
6	Whiting	Bakken	ND, US	2014	CO_2	Huff-n-puff vertical well
7	–	Bakken	MT, US	2014	Water	Flooding
8	Lightstream Resources	Bakken	SK, CA	2011	Natural gas	Flooding
9	Crescent Point Energy	Bakken	SK, CA	2006–2011	Water	Flooding
10	EOG	Eagle Ford	TX, US	2013–2015	Natural gas	Flooding

The pilots were implemented in the Bakken and Eagle Ford shales. Reservoir simulations and laboratory experiments have shown the potential of EOR program in tight formations (Hawthorne et al., 2013; Yu et al., 2018; Kovscek et al., 2008; USGS, 2013; Wan, 2015; Sheng and Chen, 2014; Sheng, 2015, Sun et al., 2016;

Tovar et al., 2014). That being said, not many major successful EOR programs have been documented (Hoffman and Evans, 2016). Several pilot tests have been implemented in the Bakken formation with CO_2 or water as injected fluids.

2.2 Operating Tight Formations

To fully appreciate the kind of research needed, it is imperative to first gain a good understanding of what tight formation typically consists of. Shale is defined as being fine-grained rock, a grain size less than 1/256 mm, porosities less than 10-13% and possessing fissility (Jiang, 2016). Shale is characterized by nano-scale pore throats (<25-30 nm, **Figure 2**), pore size distribution, and pore surface wettability partitioning (water wet versus oil-wet components). As seen in **Figure 2**, Eagle Ford shale samples are categorized into 4 groups of different carbonate concentrations. Highest carbonate samples show larger pore-throats, but poor pore connectivity; whereas, lowest carbonate samples (highest clay samples – marl stone) show smaller pore throats (Dang 2019). More importantly, the dependence of pore throat sizes as a function of mineralogy for Eagle Ford samples is illustrated. Shale is also a source rock with organic matter in its matrix, which makes flow behavior even more complicated. There are three different pore types: organic pore (generally assumed to be oil-wet), inorganic pore (generally assumed to be water-wet), and mixed-wet pores (Tinni et al., 2017) (**Figure 3**). Relative permeability for hydrocarbon and water is impacted as a function of the model distribution of the pore types. Topography results indicate micro-round pores, microcracks, and meso-

cracks (Dang, 2019). Crack features such as their density, dimension, and anisotropy are extremely sensitive to stress. This leads to shale compressibility and its associated transport properties being a strong function of geomechanical conditions (**Figure 4**, Metwally and Sondergeld, 2011).

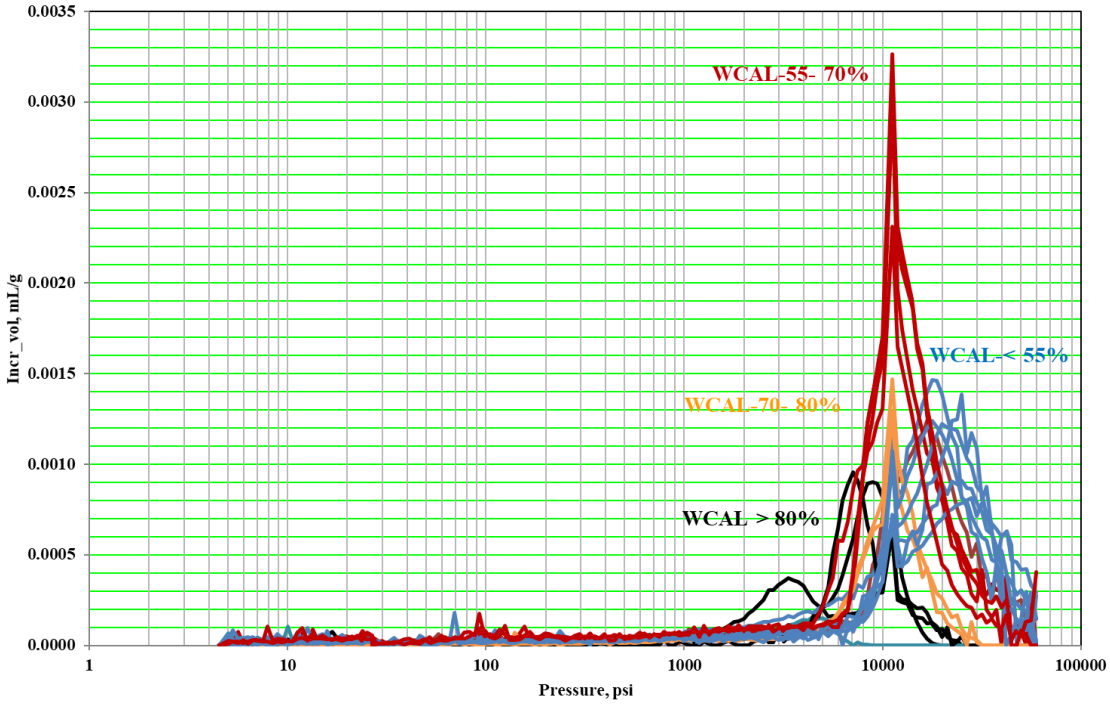

Figure 2. Examples of pore throat size distributions in the Eagle Ford shale, measured by Mercury Injection (MICP). In general, the mercury intrusion pressures for shale samples are greater than 5000 psi (Dang, 2019, data from Integrated Core Characterization Center, University of Oklahoma)

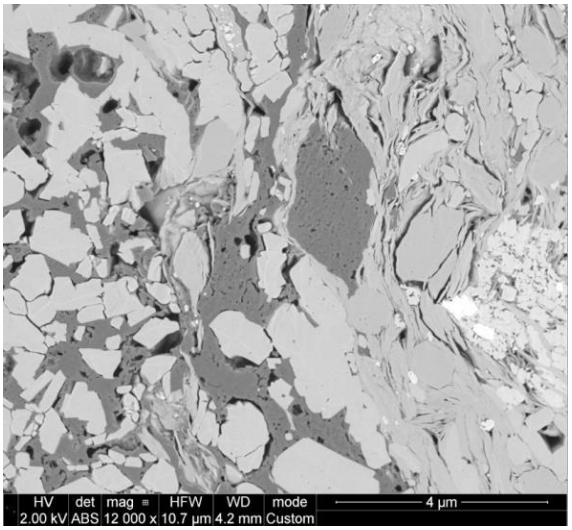

Figure 3. Back-scattered electron SEM image of an Eagle Ford sample within the oil maturity window. The bright matter is pyrite, light gray matter is mineral/inorganic matrix, and dark gray matter is solid organic content (kerogen) (Tinni et al., 2017)

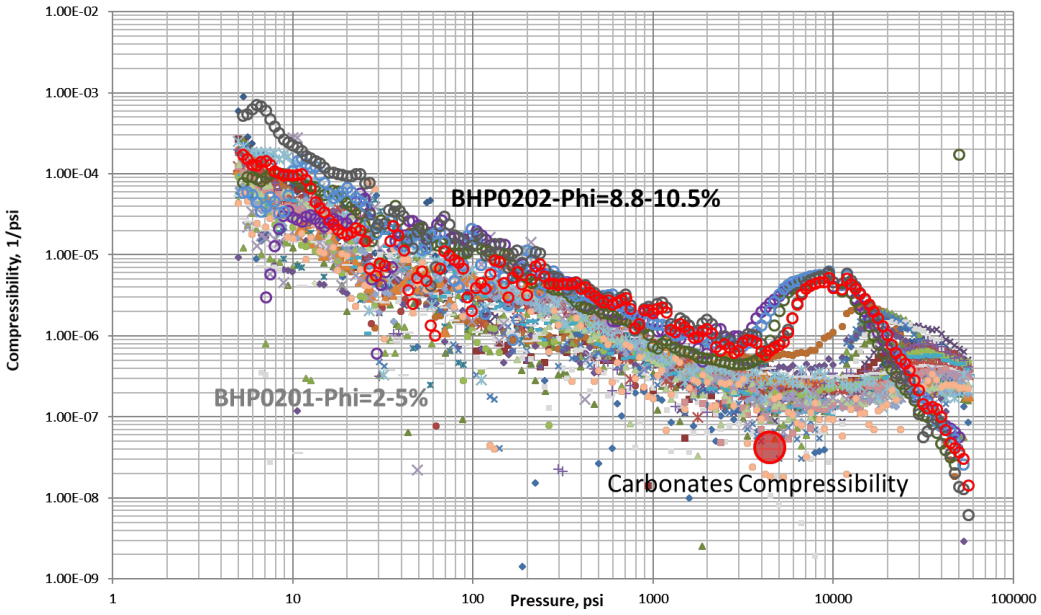

Figure 4. Effective compressibility from MICP data versus hydrostatic pressure (Dang et al., 2017)

The samples in Figure 4 above are from two different wells in the Eagle Ford, one shows higher compressibility and larger pore throats than another. Water compressibility in ambient condition is about $3.5*10\ psi^{-1}$.

Naturally occurring cracks and hydraulically induced fractures greatly affect reservoir performance; both beneficial and detrimental. A beneficial effect is discussed by Sorensen and Hamling (2016), where the high natural fracture density allows the Parshall field in the Bakken to have scientifically more crude production compared to neighboring fields. The detrimental feature, however, is the case where intensive fracture communication among offset wells, or frac-hit, in general, has a negative effect on production. Fractures thus increase the complexity of EOR projects.

The primary recovery factor is possibly in the range of 1-2 % in some of the plays in North America (Wang et al., 2016). The low percentage is due to initial high production rates, followed by a quick decline. In this scenario, the natural fractures are depleted at a much faster rate relative to the slow recharge from the rock storage matrix, due to the extremely tiny nature of the nanopores. This leads to recovery factors less than 10% (Lefever et al., 2008; Clark, 2009; Wang et al., 2015; Alvarez et al., 2016). Typical EOR simulation methods do not work with tight formations. A few examples of good candidates for stimulation in shale plays are miscible gases, surfactant, and low salinity water flooding (Song and yang, 2013; Wan et al., 2013; Wan and Sheng, 2015).

2.3 Typical Rock and Fluid Properties of Shale Plays

To get a broad overview of EOR techniques in shale, it is imperative to have a good understanding of the rock and fluid characteristics. This also helps in deciding which EOR method is more feasible to be applied. **Table 2** details said rock properties, whereas **Table 3** details said fluid properties from different resources, as compiled by Alfarge et al., (2017).

Table 2. Most common rock properties of unconventional reservoirs (Alfarge et al., 2017)

Reservoir Characteristics	Common Quality	Common Quantity	References
Porosity (%)	Low	5 - 10	SPE-178659-MS; SPE-178489-PA
Permeability (md)	Ultralow	0.0001-0.1	SPE-I68915-MS
Temperature (F)	High	240	SPE-184486-STU
Wettability	Poor	Oil wet to intermediate	SPE-179688-MS; URTeC: 2461651; SPE-153853-PA
Natural Fracture Intensity #/ft.	High	0 - 32	SPE-I689I5-MS
Grain Density g/cc	Usual	2.55-2.75	URTeC 2461651
Drive mechanism	Poor	Depletion	SPE-171668-MS
Oil Saturation (%)	Good	50-75	SPE-179533-MS
Median pore radius (µm)	Poor	0.034- 0.010	SPE-179688-MS; URTeC: 2461651
Dominant Grain Size (µm)	Tiny	<62.5	SPE-179533-MS
Total Organic Content (wt %)	Rich	0.1 to 5	URTeC 2461651

Reservoir Depths (ft.)	Deep	5045-12150	URTeC: 2433692; 21-1921 WPC
Pressure (Psi)	Abnormal	0.78	SPE-169575-MS
Bulk Density *g/cc*	Usual	2.3-2.5	URTeC 2461651
Net Thickness (ft.)	Intermediate	Oct-40	URTeC: 2433692
Formation Type	Complex	Silt, limestone, sand, shale	URTeC 1619698
Clay Content %	High	7-30%	URTeC 2461651 SPE-l 80378-MS

Table 3. Most common Fluid properties of unconventional reservoirs (Alfarge et al., 2017)

Fluids Properties	Common Quality	Common Quantity	Reference
Oil Density, API	Excellent	38-42	21-1921 WPC
Brine Specific Gravity	Heavy	1.9	SPE-171668-MS
Saturation Pressure, psia	High	2500 to 3,403	SPE-175034-MS
Contact Angle	High	81-142	URTeC 2461651
Brine TDS, (mg/I)	High salinity	228500-285,000	SPE-171668-MS SPE-178489-PA
Oil Viscosity, cP	Very low	<4.2	URTeC: 2433692; SPE-178489-PA
Total Acid Number, KOH /g	Low	0.02-0.36	SPE-171668-MS URTeC246l65I
Crude Oil Polarity	Favorable	More Paraffinic	SPE-171668-MS
Total Base Number, KOH/g	Low	0.12-116	SPE-171668-MS URTeC 2461651
PH	More Acidic	5.7	SPE-171668-MS

GOR, SCF /STB	High	507-1712	URTeC: 2433692; SPE-171668-MS
MMP for CO2, Psi	Achievable	2450 -2650	SPE-175034-MS
IFT W/O (mN /m)	High	17.2-34	URTeC 2461651

As can be seen from the table above, the most common rock criteria in most of the unconventional reservoirs of North America are low porosity, low permeability, oil-wet, high intensity of natural fractures, and wide range of mineral composition. Also, the most common fluid properties in unconventional reservoirs are high-quality oil with high API, low viscous, more paraffinic, and high GOR.

2.4 Some EOR Methods in Unconventional Plays

There are myriad methods used for stimulation in unconventional reservoirs. The ultratight matrix and high conductivity of natural fractures might be the most two important factors that impair the success of conventional EOR methods. These are Miscible Gas injection, Smart Water Flooding Technique, Chemical methods (Alfarge et al., 2017). Electrical-based techniques, ultrasonica-based methods, use of nanoparticles, among others.

2.4.1 Miscible Gas Injection:

This category has been highly researched due to its potential in tight formation EOR. Several gases have been considered for this technique, including, but not limited to, CO_2, N_2, and enriched natural gases. CO_2 typically dissolves in shale oil, swelling it up and reducing its viscosity. Also, compared to other gases such as N_2 and CH_4, CO_2 has a lower miscibility pressure with shale oil (Zhang et al., 2016). Due to these, and other reasons, CO_2 has been a big focus of research. Co_2 driving mechanisms are as follows; diffusion mostly from lab work, reduction in capillary forces, repressurization, oil swelling and pressure maintenance, oil viscosity reduction and some combination of all the stated mechanisms.

That notwithstanding, the minimum miscibility pressure of CO_2 in these types of oil has a controversial range between 2500 psi to 3300 psi (Alfarge et al., 2017). A model in which gas is injected into a hydraulic fracture along a horizontal well was built by Zhu et al., (2015). Substantial improvement in oil recovery was realized in this study by injecting CO_2 in reservoirs with fluid flow from fracture to fracture.

Hoffman et al. (2016) show that earlier modeling methods in continuous gas flooding recovered 10-20% of oil in place, whereas huff-n-puff contributed to about 5-10% (2016). A model involving capillarity and adsorption effect of the

small pores for shale reservoirs was introduced by Pu et al., (2016), in an attempt to properly simulate EOR CO_2 in an unconventional reservoir. But more importantly, including capillarity in the modeling process typically predicts higher oil recovery.

2.4.2 Smart Water Flooding Technique:

The effects of Low Salinity Water (LSW) flooding on EOR has been investigated. Currently, the issue of the underlying mechanisms which are behind wettability alteration is still a topic of debate. Understandably, wettability alteration is driven by double-layer expansion and multicomponent ion exchange due to the addition of salt, and interfacial tension might be the main mechanism for LSW flooding. LSW driving mechanisms are as follows; Shale cracking, osmotic effect, wettability alteration by ionic layer, and changing pH (Alfarge et al., 2017).

2.4.3 Chemical Technique

Surfactant, polymer, and alkaline methods typically make up this category (for shales). Surfactant has the most promising potential to improve oil recovery in these reservoirs. Multiple investigations have been conducted on surfactant for EOR shales (Wang et. al., 2011; Wang et al., 2012; Dawson et al., 2015), and it has shown to be the most promising potential for tight formation EOR. Experimental work was conducted on how surfactant could enhance oil recovery in the Bakken, with results being upscaled through numerical simulations (Dawson et

al., 2015). Alvarez et al., (2014) discovered that surfactant can lower contact angle, making a system more water wet, and thus improving oil recovery. Further investigation into the effects of multiple surfactant types on interfacial tension and contact angle by using basin cores was conducted by Alvarez et al., (2016). Surfactant mechanics are as follows; Wettability alteration, reducing IFT and enhancing water imbibition.

Very little work has been conducted with alkaline and polymer in these reservoirs. This could be because of the associated issues with injectivity, although conformance problems are more dominant in the reported pilot tests (Hoffman, 2016).

2.4.4 Electrical-based, Ultrasonic and Nanoparticle Methods

Electrical heating techniques are utilized to improve heavy oil recovery, which is approximately 70% of total reserves in the world (Mozafari and Nasri, 2017). These methods increase the oil temperature by exciting the hydrocarbon molecules through electromagnetic heating and ultrasonic stimulations, causing a reduction in viscosity (Shafiai, 2020). Electromagnetic heating is a way to transmit heat to the reservoir to raise its temperature, with minimal heat loss to the. This method could be deployed in regions with permafrost, where it will be difficult to perform traditional EOR techniques in those environment. Ultrasonic methods also help greatly improve rate of recovery, and doesn't contaminate the oil layer. They are great for heavy oil reservoirs and low-permeability reservoirs, however, even

though it shows promise, it is currently not being used in the field, and is still being developed in labs (Wang, 2020).

Furthermore, nanoparticles in the form of nanofluids, nano-catalysts, and nano-emulsions have been considered as potential agents to EOR. Parameters such as the injection rate, concentration of nanoparticles, size, temperature and type of nanoparticles all have significant effects on the performance of nanofluid flooding (Ali et al., 2020). Phenomenon such as IFT reduction, wettability alteration, and viscosity modification are some of the ways that enable the application of nanoparticles for improving oil recovery. Thus, it is highly imperative to understand the mechanisms of these phenomena for enhanced oil recovery is much needed to improve recovery factor from EOR (Ali et al., 2020).

2.5 Addressing the Discrepancy between Test Scales

Hoffman et al., 2016 present that CO_2 is outperformed by natural gases in pilot tests, based on EOR case studies reported. This, however, is inconsistent with research from lab and simulation modeling data, (as CO_2 is the most successful EOR technique **Figure 5** below), and this means that a discrepancy exists between pilot tests and lab work for CO_2 injection. This also means that the underlying mechanism for field-scale CO_2 isn't well understood. Alfarge et al., (2017) mention that upscaling the proposed lab mechanisms for CO_2 such as diffusion mechanism

and diffusion rate to the field scale by specifying these exact values is misleading way and more optimistic at the same time.

Directly upscaling CO_2 lab results to filed scale is problematic as most experimental conditions utilize very small core chips of Bakken or other formations for study. Moreover, the time exposure of these chips is in the range of 96 hours, and this increases oil recovery (Hawthorne et al., 2013). Thus, long exposure time and large contact area are needed if results are to be directly upscaled to be comparable. Possible explanations could be that either the oil recovery process is too fast or CO_2 diffusion rate in field conditions are extremely slow (Alfarge et al., 2017)

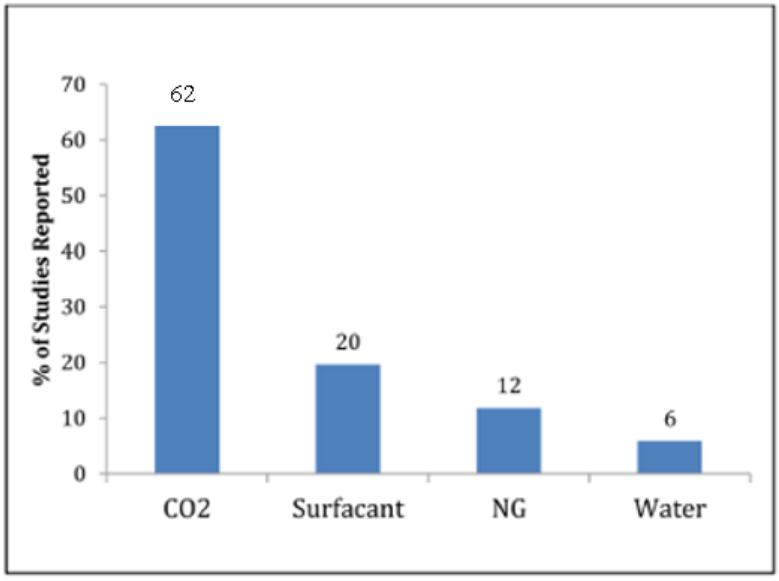

Figure 5. The most potential IOR methods in ULR (Alfarge et al., 2017)

Dang (2019) presented a novel technique that allowed the combination of two techniques to continually estimate the incremental recovery factor without removing the rock specimen from a test chamber. His work details the fact that the EOR agent will not go very far into the matrix, unless a large diffusion coefficient is used. His work assumes a network of fractures, where gas is diffused from the many small, tiny fractures to the matrix. However, this work views the entire system as a lumped, high permeability system, where the entire fracture network fracture distribution is unknown. This is of course a simplification, however, its' a simpler, easier way to view the problem.

For tight formations, a small diffusion coefficient must be used, and the distribution of the matrix and fracture network must be known, which not the case is. This information could however, be determined through experiments or numerical simulations.

Chapter 3 Methodology

3.1 Mathematical Modeling of Huff-n-Puff

In this section, miscible gas recovery (huff-n-puff scheme) from the shale matrix using transient linear model is evaluated and compared. Mass flux for linear configuration under transient conditions to represent gas flow toward matrix during injection and soaking period and from the matrix during the production stage is calculated. The injection pressure is assumed to be larger than minimum miscibility pressure (MMP); hence, it can assume that a single-phase tracer flow would mimic the process. The BHP during the production stage, in practice, is smaller than MMP and thus two-phase flow would occur. However, it is assumed that a dynamic decrease in diffusion/dispersion coefficient during the production stage (for simplicity, we consider a linear equation would capture mass flux reduction with time due to two-phase phenomena in the shale matrix (Yuan et al., 2017). Also, for purposes of this model, we assume there is no water interaction within the system. **Figure 6** represents a schematic of one of the fracture stages from the stimulated matrix and in this model, linear flow between matrix and induced fractured area is considered. For the injection stage, the geometry of fracture stages may be considered as plane sheets and an equation of Fick's second law can be solved for chosen initial and boundary conditions (Davudov et al., 2016a; Davudov et al., 2016b). However, for the soaking and production stages, the geometry of fracture

stages may be considered as slabs with finite volumes, and heat diffusion equations with limited volume can be solved for the non-uniform initial condition created at the end of injection (and consequently after soaking). Our model utilizes the diffusion-dominant mechanism, as will be seen in the equations below. The diffusion mechanism is well studied and understood as, Kovscek et al., 2008, Vega et al., 2010, Hoteit et al., 2011, Chen, et al., 2014 and Alharthy et al., 2015 all discuss the diffusion-driven IOR mechanism in their work.

3.2 Modeling Stages

As discussed earlier, there are three main stages for this model; injection, soaking, and production, as seen in Figure 6. In the first stage, there is the injection of CO_2 into the fractured system at a pressure of 2000 psi, and at a temperature of 150^0 F. Final constant pressure value of 3500 psi is used as the minimum miscible pressure value corresponding to the C_{inj} parameter in **Eq. 8** below. This allows the gas to flow from the fracture and contact the reservoir at some penetration length, as seen by the green drops moving into the matrix in **Figure 7**. We observed counter-current diffusion during the injection stage, and this is seen as the red drops moving away from the matrix in Figure 7**.** When simultaneous injection/soaking and production occur, this is considered counter-current, and when it occurs in series, it is called co-current (Alfarge, et al., 2017). This thesis only focusses on the co-current phase.

For the second stage, there is a wait time, during which the gas can permeate the matrix. This is termed the soaking stage. The gas in the system diffuses through the matrix to increase the contact region with the matrix. This stage is also marked by a counter-current diffusion, as seen in Figure 7. As will be seen later in this thesis, the soaking stage is significantly affected by a $V_{fracture}$ to V_{matrix} ratio. CO_2 is known to have very good miscibility with oil, and thus is very effective for EOR gas injection (Alfarge et al., 2017).

Thereafter, there is the final stage, where the gas is produced back. The gas binds with the oil, decreasing its viscosity and increasing its mobility within the matrix. This marks the end of the 3 stages, however, there is still some residual gas with the system, which contacts the entire matrix at infinite time. This phenomenon is not accounted for in our model since real operations in the field are bound by specific time schedules.

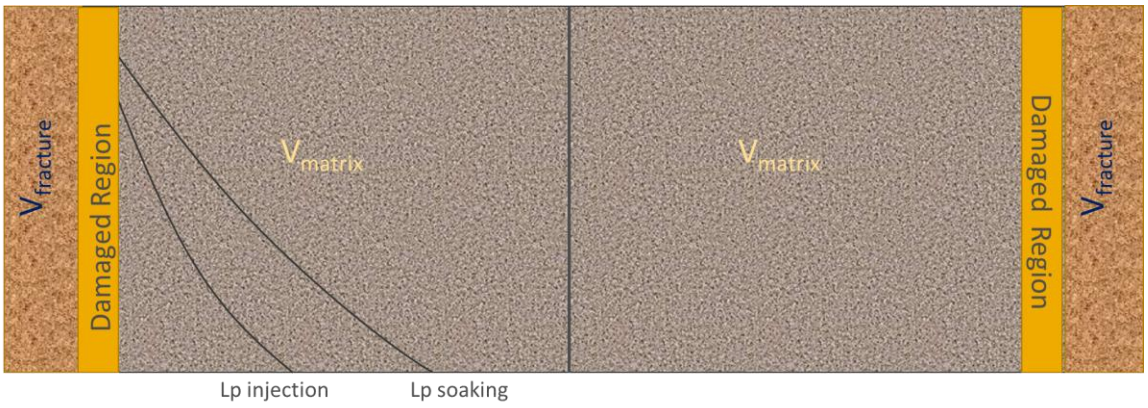

Figure 6. Injection and Soaking Profile Schematic

Modeling Assumptions

- Single-phase isothermal (P>MMP); two-phase causes a reduction in available space for oil (the effect is absorbed by the Biot number)
- Pressure drop causes pore connectivity loss, leading to a reduction in permeability and conductivity
- Water interaction in the system is not considered
- The diffusion coefficient of the miscible mixture of the oil and gas is 10 times less than the miscible agent (CO_2), to correct for neglecting two-phase flow.

3.3 Modeling Equations

The mass balance equation for the shale matrix can be written as:

$$\phi \frac{\partial \mathrm{C}}{\partial \mathrm{t}} + (1-\phi)\frac{\partial \mathrm{C}_\mu}{\partial \mathrm{t}} = \Gamma \phi D_t \frac{\partial^2 \mathrm{C}}{\partial \mathrm{x}^2} + \Gamma(1-\phi)\, D_s \frac{\partial^2 \mathrm{C}_\mu}{\partial \mathrm{x}^2} \qquad (4)$$

Where ϕ porosity, C is the amount of free gas, C_μ is the surface concentration of adsorbed phase in kerogen, Γ is interconnectivity term which used in place of tortuosity, D_s is the surface diffusivity of the adsorbed gas in the kerogen, and D_t is total effective pore diffusion coefficient including molecular diffusion and Knudsen diffusion (Moghanloo et al., 2013).

D_t can be expressed as:

$$D_t = \omega D_f + (1-\omega) D_\kappa \qquad (5)$$

Where D_f is Fickian diffusion, ft^2/s D_k is Knudsen diffusion ft^2/s and ω is a weighting factor. Following Wu et al., (2014), it can be estimated as a function of the Knudsen number as $\omega = 1/(1+Kn)$. Furthermore, if Henry's law of linear

relationship is assumed for gas and adsorbed phase concentrations, C_μ can be expressed as KC, where K is Henry's constant. Based on the discussed assumptions above, **Eq. 4** can be rewritten as:

$$\frac{\partial C}{\partial t} = D_t \frac{\partial^2 C}{\partial x^2} \tag{6}$$

Where D_T can be formalized as:

$$D_t = \Gamma \frac{\phi\left(\omega D_f + (1-\omega) D_\kappa\right) + (1-\phi) K D_s}{(\phi + (1-\phi) K)} \tag{7}$$

Following Crank's book, concentration is solved based on the plane sheet model, to obtain the following expression at different injection time. Since the EOR agent is being injected from outside into the system, this model allows to study the diffusive flow into a system, just as diffusion happens along a sheet.

$$C_{inj}(X,T) = C_0 + (C_1 - C_0)\left(1 - \frac{4}{\pi}\sum_{n=0}^{\infty} \frac{(-1)^n}{2n+1} \exp\left\{\frac{-D_t(2n+1)^2\pi^2 t}{4L^2}\right\} \cos\left[\frac{(2n+1)\pi x}{2L}\right]\right) \tag{8}$$

Following Mikhailov and Ozisik's book, concentration is solved based on the slab model, to obtain the following expression at different soaking and production times. This is because when the EOR agent is in the system, there is finite volume, which the slab model is consistent with.

$$C_{soak}(X,T) = \frac{\theta_0 + K\int_0^1 X^{1-2m}F(X)dX}{1+K/[2(1-m)]} - \sum_{i=1}^{\infty} E_i \left[\theta_0 - \mu_i \int_0^1 X^{1-m}\,\frac{J_{-m}(\mu_i X)}{J_{-m}(\mu_i)}F(X)dX\right] \frac{X^m J_{-m}(\mu_i X)}{J_{-m}(\mu_i)} e^{-\mu_i{}^2\tau} \quad (9)$$

$$\tau = \frac{D_t(T-T_1)}{L^2} \quad (10)$$

$$C_{prod}(X,T) = C_{soak}(X,T)\ @\ \tau = \frac{D_t(T-T_2)}{L^2} \quad (11)$$

where C_{inj} is the amount of moles of gas injected into the system, C_0 and C_1 are the initial and final molar concentrations, in mole/ft.^{3}, D_t is the diffusion rate, in ft^2/s, L is the half fracture spacing in ft., T is time, in seconds, x is a length variable, in feet, C_{soak} is the amount of moles of gas per ft^3 infiltrating the system, X is the dimensionless length, x/L, C_{prod} is the molar concentration per ft^3 of gas produced, K is the ratio of the volumes of matrix and fracture network, μ_i values are the non-zero positive roots of $\tan q_n = -\alpha\, q_n$ (Crank, 1975), where $\mu_i = q_n$. F(X) is a function of the initial condition profile after the injection phase for C_{soak}, and a function of the initial condition profile after the soaking phase for C_{prod}.

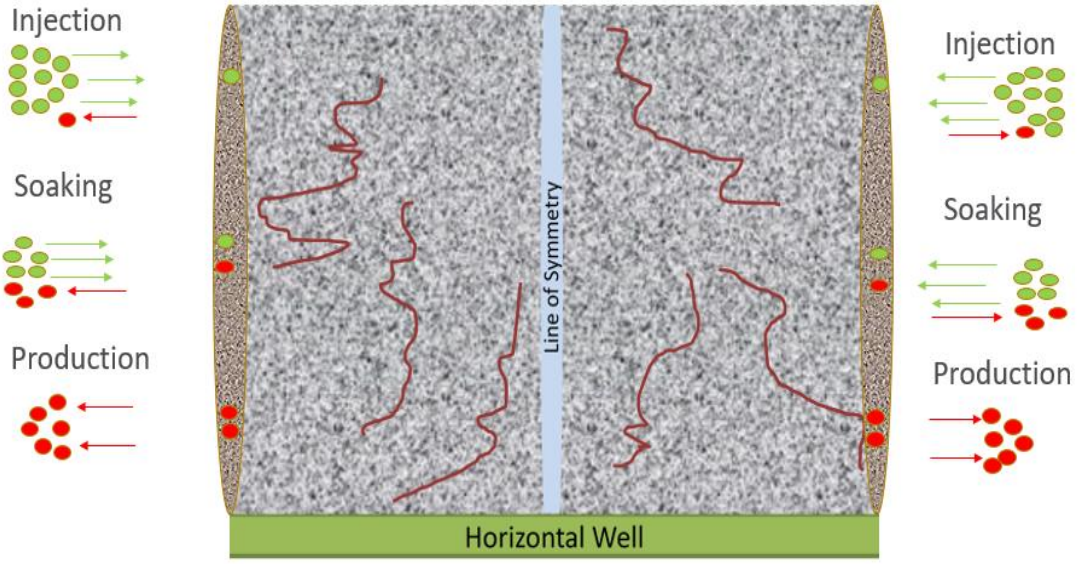

Figure 7. Schematic of linear flow from stimulated matrix toward fractured area. Green circles represent injected gas and red circles represent produced oil (Moghanloo, 2013).

We hypothesize in this project that the choke effect can be explained by loss of interconnectivity within the porous medium with pore pressure drop (increased effective stress and/or two-phase phenomena). We then verify it with experimental work and model it with a dynamic reduction of diffusion coefficient, as shown later in the results section. We ran various sensitivity analyses for the effect of different input parameters on the recovery factor, which is defined as the total moles produced to the total molar intake of the system. Interestingly, lab-scale recovery is a function of pressure drawdown during production (choke effect). The speed at which gas and vaporized oil components will be produced back after soaking time is controlled by choke-size.

3.4 Experimental Procedure

Experiments were run in the Integrated Core Characterization Center, and the data was used in this study to get an idea of how the cycle speed affected recovery. Prior to the EOR experiments, approximately 50 g of the Eagle Ford shale sample were crushed and sieved to an average particle size of 7.5 mm. Approximately 14 g of crushed samples was used for every set of Huff n' Puff experiments. **Figure 8** illustrates the experimental setup used for these experiments. The pressure vessel containing the crushed samples was heated to a temperature of 150 ^{o}F for 1 hour before CO_2 injection. For every cycle, CO_2 was injected in the pressure vessel until the pressure reached 3500 psi. The CO_2 pressure of 3500 psi was maintained by the metering pump for 5 minutes in order to stabilize the system at 150 ^{o}F. The stabilization step was followed by a wait or soak time of 1 hour. During the soaking period, all valves (2 and 3) that allowed a connection to the pressure vessel were closed. After the soaking period, the system was depressurized. Two depressurization rates were tested. During the first set of Huff n' Puff experiments, the system was depressurized from 3500 psi to atmospheric pressure in 3 minutes while for the second set of experiments the pressurization step lasted 45 minutes. After depressurization, the samples were removed from the pressure vessel and cooled to room temperature in a desiccator for 1 hour. The amount of fluid produced from the samples during every cycle was obtained by computing the difference

between the NMR volumes measured before and after every cycle. The NMR measurements were conducted at 12 MHz and a TE of 0.114 ms.

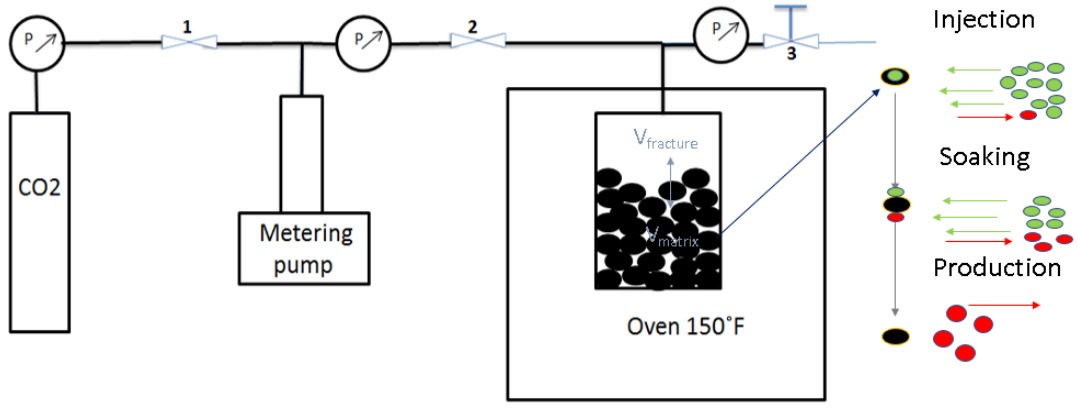

Figure 8. Experimental setup used to perform the Huff n' Puff experiments. Valve 3 is a needle valve that can be used to control the depressurization rate.

3.5 Modeling Procedure

Using **Eqs. 8-11,** a simulation is created to study EOR optimization. In this model, Lp is determined from the fracture half-length. Through a series of steps, the individual parameters in the equations are calculated for values ranging from 0 to 2000. Concentrations are calculated based on the coefficient of the plotted curve of a parameter set profile. After an injection phase, a soaking phase follows, where some volume of gas is now available within the fracture to penetrate the matrix. Thereafter, concentration is set within the fracture, and observations on rate and cumulative productions coming out of the matrix are made, resulting in the

generation of recovery factors. These are the ratio of produced moles to intake moles by the system.

The diffusion coefficient is assumed to follow the relationship in **Eq. 12** below, where the choke effect parameter, b, affects production.

$$D_t = D_{matrix}\left(1 + be^{-\lambda t}\right) \quad (12)$$

Where D_t is the total diffusion rate, ft^2/s, D_{matrix} is the initial diffusion rate, ft^2/s b is the parameter which quantifies the so-called choke effect during production, and it is time variable. For the injection and soaking stages (Eqs. 8 & 9), b is 0, thus, $D_t = D_{matrix}$. For the production stage, however, D_t decreases by an order of magnitude, thus, from 10^{-10} to 10^{-11} ft^2/s for instance, due to the choke effect, where $b \neq 0$. This phenomenon is strongly observed on the lab scale, where the connectivity loss is almost instant as the pressure wave propagates instantaneously throughout the small system. On the field scale, however, this choke effect happens mainly at the fracture-matrix interface. It also happens within the matrix itself and explained as a loss in connectivity. This is however taken care of by the Biot number.

3.5.1 Biot number, Bi

Biot number is a dimensionless group that compares the relative transport resistances, external and internal. It arises when formulating and non-dimensionalizing the boundary conditions for the typical conservation of species/energy equation for heat/mass transfer problems (Adrian, 2007) The Biot number is explained as the resistance of fluid moving from outside the system to

inside the system. Therefore, this resistance quantifies the loss in connectivity, capillary pressure changes, two-phase phenomenon, and other scale parameters absent on the lab scale, but present in the field. The use of this number allows for similar equations to be used on both lab and field scales while accounting for scale differences.

We defined the Biot number as:

$$\frac{1}{Bi} = \frac{A_c D_t}{V_{matrix} k_{fracture}} \tag{13}$$

Where A_c is the contact area between the fracture network and the matrix, D_t is the total gas diffusion coefficient in the matrix, V_{matrix} is the matrix volume and $k_{fracture}$ is the fracture permeability, mD.

3.5.2 Penetration Length, L_p

The gas only goes so far into the matrix when injected. Thus, arises the need to determine a penetration length. A penetration length that provided a C_{inj} concentration of 1%, was calculated, as this was determined to be the penetration minimum threshold value below which our equations were valid. This was determined for given constant L, t, and D values. Due to how this parameter was quantified, it was seen that penetration length values, L_p, were most sensitive to the total system half-length, L, the diffusion coefficient, D and the time of injection/soaking. Also, the L_p is a representation of DPV, which provides the

accessibility factor value to scale our results.

For the injection phase, a diffusion front is determined at different values of x length in the system. Thereafter, based on the injection L_p, and the profile of the diffusion front after injection, a new L_p is determined for the soaking phase. This is calculated as the length at which C_{soak} becomes 1% within the system. At this stage, another profile for the diffusion is determined using Eq. 9 and used as input for the production stage. The L_p from the soaking stage and diffusion profile are used to determine the concentration within the system after some time, T_2 using Eq. 11.

Two recovery factors are then calculated as recovery efficiencies. The first being the ratio of the cumulative production to the cumulative gas in the system after production. This recovery value is then multiplied by the (dimensionless) length of the entire system, to obtain the second recovery efficiency. This gives the recovery for the entire system. Evaluating recovery this way provides a systematic approach of upscaling the results and helps to give some prediction of what actual field recovery efficiencies might be.

3.6 A Theoretical Explanation of the Choke Effect

Shale resources illustrate distinct characteristics, such as micro-scale pores (IUPAC definition), ultra-low permeability, and complex pore network system. One of the key parameters in shale formations is pore connectivity. Hu et al., (2012) have reported very low connectivity for Barnett samples based on three experimental

approaches (imbibition, tracer concentration profiles, and imaging) they have conducted. Davudov and Moghanloo (2016) and Davudov et al., (2016b) also studied connectivity in shale formations based on mercury injection capillary pressure (MICP) data, which they have reported that the percentage of accessible pores in Barnett and Haynesville shale fields is around 30%. This loss of connectivity is generally termed choke effect, as observed in **Figure 9** below.

Recently, Davudov and Moghanloo (2018) have proposed to formulate interconnectivity parameter (Γ), as a function of coordination number/average pore throat number, z as:

$$\Gamma = \exp(-\eta/z) \tag{14}$$

Where $\eta = \frac{4}{3-D_{fr}} + 4$ with D_{fr} being fractal dimension.

By further evaluating experimental data, Davudov and Moghanloo (2018) have suggested that connectivity loss (coordination number reduction) is one of the major reasons for the reduction in matrix deliverability/hydraulic conductivity as a function of effective stress. In one of the samples studied, they have shown a 50% reduction in coordination number which corresponds to more than 95% interconnectivity, Γ decrease as shown in Figure 9.

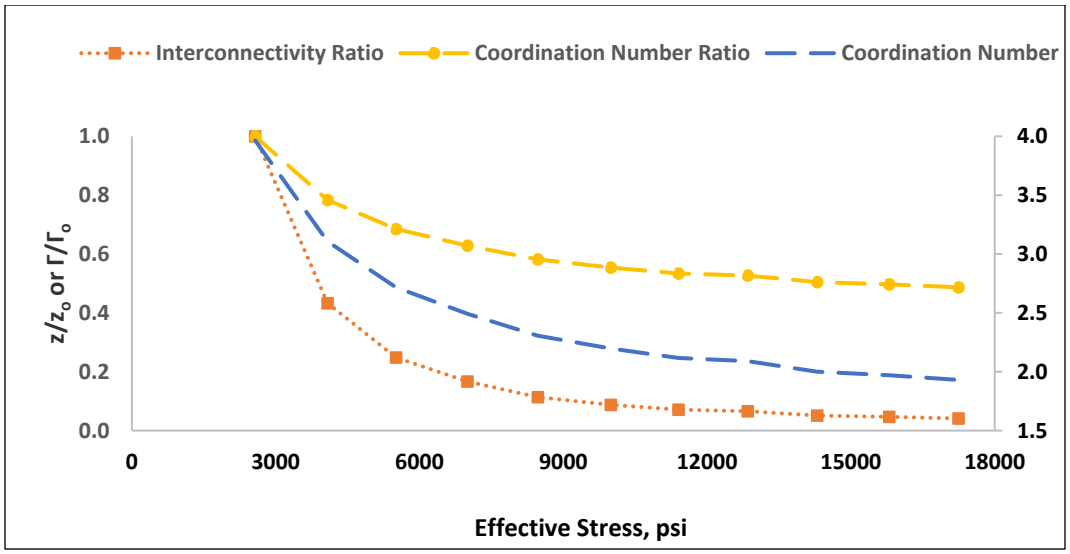

Figure 9. Interconnectivity parameter and coordination number as a function of effective stress for shale samples (Davudov and Moghanloo 2018).

3.7 Upscaling of EOR Results; Discrepancies between Prediction and Pilot Observations

As discussed earlier in this thesis, we propose a systematic way of scaling results from the lab to the field scale. We do this by lumping all the unknown parameters into a Biot coefficient, and taking the loss of interconnectivity into account, as a "b" parameter (choke effect). The fracture volume in the lab is much larger than the matrix volume, and vice versa for the field. This means a scaling model approach should account for this. **Figure 10** depicts this ratio difference on both scales.

To account for the scale difference, we vary the values of E_i in **Eq. 15**. E_i is calculated as:

$$E_i = \frac{2}{\mu_i}\left[1 + \frac{2m}{\mu_i}\left(\frac{\mu_i}{Bi} - \frac{K}{\mu_i}\right) + \left(\frac{\mu_i}{Bi} - \frac{K}{\mu_i}\right)^2 + \frac{2K}{{\mu_i}^2}\right]^{-1} \quad (15)$$

Where m = 0.5 for a slab, Bi is the Biot number, K is the ratio of the volumes of matrix and fracture network, μ_i values are the non-zero positive roots of $\tan q_n = -\alpha\, q_n$ (Crank, 1975), where $\mu_i = q_n$

Furthermore, pressure drop change on the lab-scale occurs at an almost instant rate throughout the system, while it takes a much longer time for pressure changes to reach the system boundary for the field scales. The results from work done by Yuan et al., 2017 show that it takes almost a year for the pressure waves created at production wells in Niobrara formation to reach the external boundary. Therefore, it would take a much longer time for the injected fluid to cover the inter-well spacing and thus the recovery factor (if defined in terms of inter-well spacing) will be very small. This is a scale discrepancy which is addressed by the Biot number in our model.

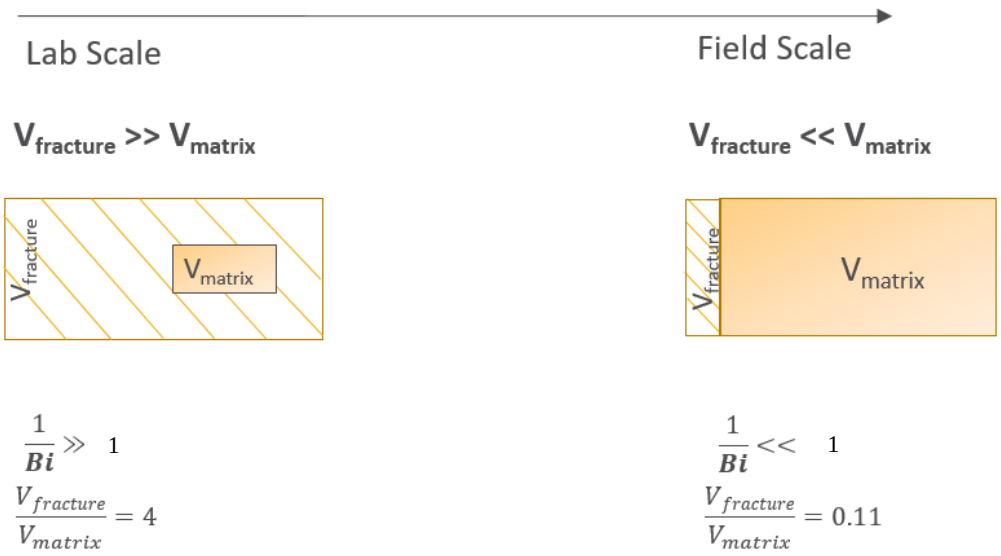

Figure 10. Upscaling schematic, depicting different Bi and fracture to volume ratios

Figure 11 shows the concept of Dynamic Drainage Volume (DDV). The four red-coated bars at the bottom of the diagram are fracture clusters. Here, smaller time represents smaller clusters, and larger time, represents larger clusters. Thus, it takes time for the pressure to propagate throughout the system. The results have been obtained using an in-house developed simulator: OUWELL.

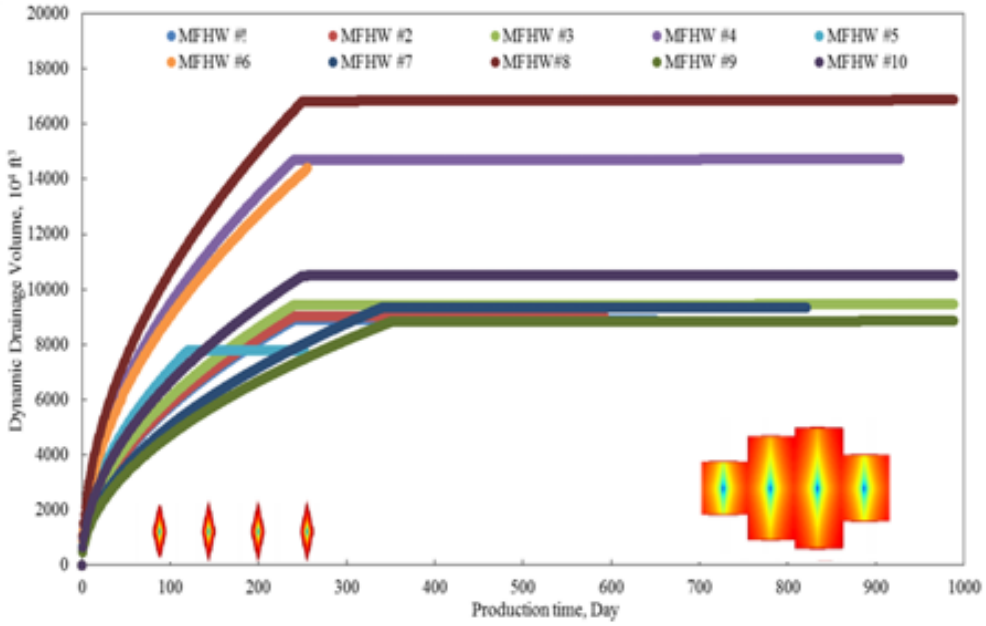

Figure 11. DDV as a function of time for Niobrara formation (adopted from Yuan et al., 2017)

The results showing that it takes almost a year for the pressure waves created at production wells in (Niaborora formation) to reach to the external boundary; therefore, it would take a much longer time for the injected fluid to cover the inter-well spacing and thus the recovery factor (if defined in terms of inter-well spacing) will be very small.

Chapter 4 Results and Discussions

4.1 Experimental Results

From **Table 4**, it can be seen that for different cycles, we get a rate ratio of about 2. This means that there is about twice as much production at a slower rate than there is at a faster rate. Thus, if one produces too fast, one may lose a valuable recovery percentage. We tried to verify this experimental result by simulating the first cycle. We theorized that the difference in these recovery factor rates is possibly due to the choke effect, and the presence of two-phase fluids in the system. Our simulation doesn't capture the two-phase fluid behavior, however, it verifies the effect of b values on recovery factors, thus, providing some evidence for the choking effect during production. We observed from experimental results that indeed the choke effect exists and, the EOR recovery in shale formations is a function of how fast we produce: the slower the production, the larger the recovery.

Table 4. Results of Experimental Data

Recovery (%)			
Cycle #	Fast Flow rate	Slow Flow Rate	Slow/Fast Rate Ratio
1	12	27	2.250
2	24	44	1.833
3	28	55	1.964
4	30	61	2.033
5	31	64	2.065

4.2 Modeling Results

The corresponding quantity in the system after infinite time following injection time is given as:

$$\frac{M_t}{M_\infty} = 1 - \sum_{n=0}^{\infty} \frac{8}{(2n+1)^2\pi^2} \exp\left\{-\frac{D(2n+1)^2\pi^2 t}{4l^2}\right\} \quad (16)$$

where M_∞ is the amount of moles of gas left in the system, M_t is the amount of moles of gas left in the system after time t, D is the diffusion rate, in ft^2/s, l is the half fracture spacing in ft. and it is time, in seconds.

The experimental procedure shows that indeed the choke effect takes place. As the rate of production increases, the total recovery rate decreases, so one loses production in the long run. We performed a series of sensitivity tests to analyze the effect of the input parameters on recovery efficiency. We defined recovery efficiency as the ratio of produced moles to moles intake absorbed by the system (since not every mole of injected gas is absorbed). We performed a sensitivity analysis on the fracture to matrix volume ratio, the Biot number, and the diffusivity coefficient to examine their effects on recovery efficiencies. The results are shown below.

In **Figure 12** below, the field scale results are represented for $V_{fracture}/V_{matrix} = 0.11$. When the field condition 1/Bi=0 is applied (yellow curve), the displacement efficiency, $E_{displacement} = 0.53$, and total efficiency, $E_{total} = 0.023$. When the lab

condition 1/Bi=100 is applied (red curve), displacement efficiency, $E_{displacement}$ = 0.58, and total efficiency, E_{total} = 0.025

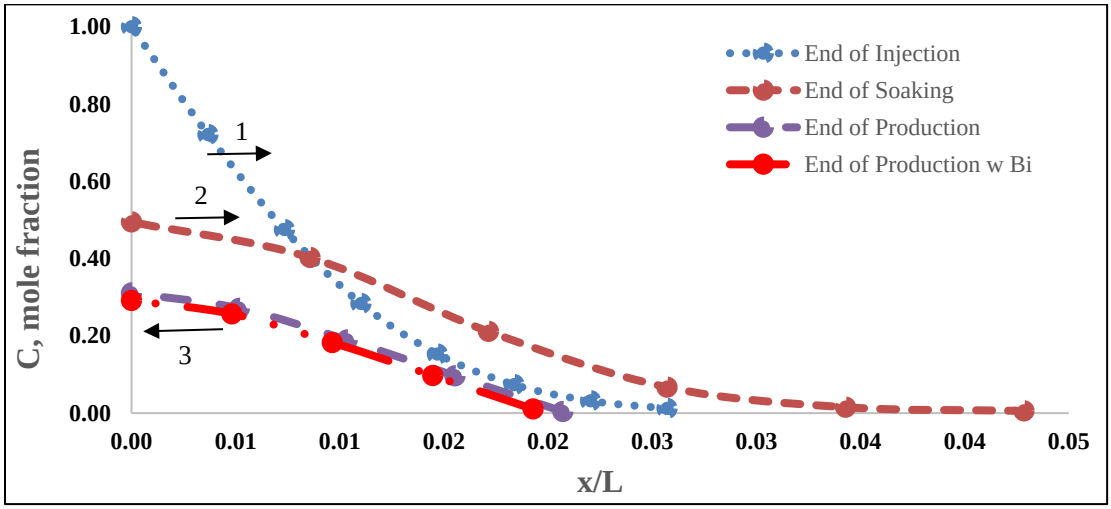

Figure 12. Representation of field scale. Vfracture /Vmatrix = 0.11

In Figure 12 above, 1 represents injection, 2 represents soaking and 3 represents production. In **Figure 13** below, the field scale results are represented for $V_{fracture}$ /V_{matrix} = 0.43. When the field condition 1/Bi=0 is applied (yellow curve), the displacement efficiency, $E_{displacement}$ = 0.47, and total efficiency, E_{total} = 0.02. When the lab condition 1/Bi=100 is applied (red curve), displacement efficiency, $E_{displacement}$ = 0.61, and total efficiency, E_{total} = 0.026.

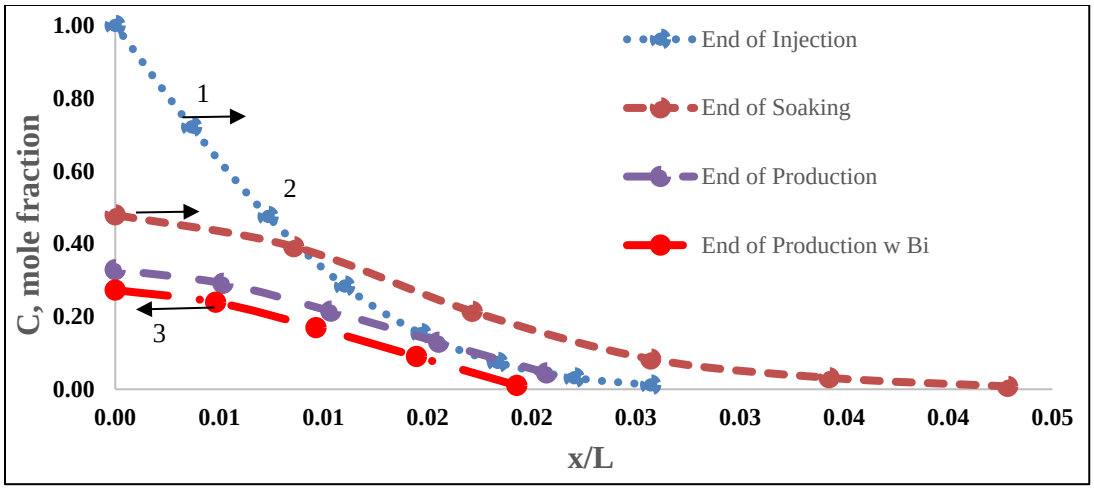

Figure 13. Representation of field scale. Vfracture /Vmatrix = 0.43

In Figure 13 above, 1 represents injection, 2 represents soaking and 3 represents production. In **Figure 14** below, the field scale results are represented for $V_{fracture}$ /V_{matrix} = 4. When the field condign 1/Bi=0 is applied (yellow curve), the displacement efficiency, $E_{displacement}$ = 0.15, and total efficiency, E_{total} = 0.006. When the lab condition 1/Bi=100 is applied (red curve), displacement efficiency, $E_{displacement}$ = 0.61, and total efficiency, E_{total} = 0.025.

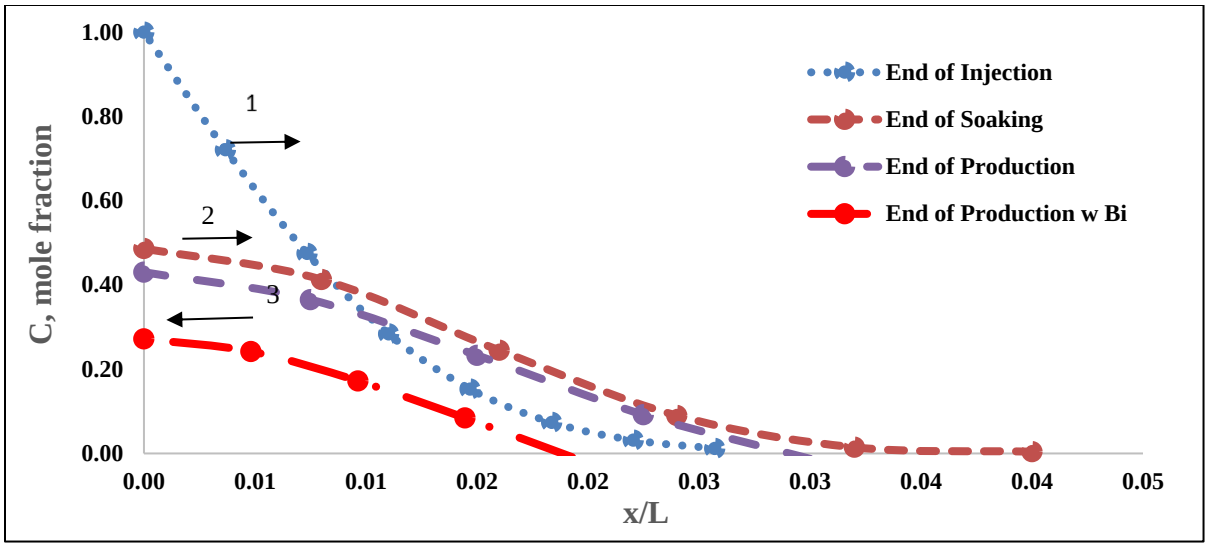

Figure 14. Representation of lab scale. Vfracture /Vmatrix = 4

In Figure 14 above, 1 represents injection, 2 represents soaking and 3 represents production.

4.2.1 Effect of Diffusivity Coefficient (DT/L^2):

This parameter captures the effect of D, L, and T in the model. L is not of much interest, even though sensitivity studies is done on it. D from literature is about 1*10^-7 ft./sec^2 unit (Zou, 2015). This is a critical parameter, as it affects the rate at which CO_2 diffuses into the formation. T is of much interest to researchers and practicing engineers alike. Optimization of this parameter is done in this work, the diffusion coefficient, time and fracture half-length are held constant and each parameter is varied for analysis.

Sensitivity analysis was done on different values of diffusivity coefficient, Dt/L^2, to obtain recovery efficiency values. These efficiencies were determined for a

constant $V_{fracture}/V_{matrix}$ value of 0.11 (field scale) and displayed in **Table 5** below. Total efficiency is calculated from displacement efficiency using the relation in **Eq. 16.**

$$E_{tot} = E_{displacement}\, x\, Accessibiliy\ factor \quad (16)$$

Multiplying displacement efficiency by the accessibility factor, (defined in Eq. 3) provides a systematic approach of upscaling the results and helps to give some prediction of what actual field recovery efficiencies might be. The accessibility factor determines the fraction of original oil contacted at any given time and, in a way, is a manifestation of volumetric sweep efficiency used in conventional reservoirs. The accessibility factor grows with $\sqrt{time}$.

Table 5. Results of simulation data for Vfracture/Vmatrix = 0.11

	Lab Scale 1/Bi = 100			Field Scale w 1/Bi = 0	
Dt/L^2	L_p	$E_{displacement}$	E_{tot}	$E_{displacement}$	E_{tot}
5.3E-03	26	0.487	0.181	0.427	0.159
5.3E-04	9	0.561	0.072	0.498	0.064
5.3E-05	2.8	0.606	0.024	0.558	0.022

It can be seen from the results above that penetration length, L_p significantly decreases as diffusitivity parameter (Dt/L^2) decreases, resulting in smaller accessibility factors. Even though the displacement efficiency values increase, the more important parameter, total efficiency, decreases. This occurs because of the decreases in the accessibility factor. When the lab condition is applied to the results,

slightly higher efficiency values are obtained, as compared to when field condition is applied to the results. This is explained by the difference in contact area from lab to field, where the gas is in much more contact with the matrix on the lab scale and has less contact with the matrix on the field scale. The differences here are not, however, staggering because of the complex effects of the diffusivity coefficient on the results. That notwithstanding, from Table 5, total efficiency is seen to significantly be a function of the diffusivity coefficient.

4.2.2 Effect of $V_{fracture}/V_{matrix}$

Sensitivity analysis was done on different values of $V_{fracture}/V_{matrix}$ to obtain recovery efficiency values. These efficiencies were determined for a constant diffusivity coefficient value of 5.3E-03 and displayed in **Table 6** below.

Table 6. Results of simulation data for Dt/L^2 of 5.3E-03

	Lab Scale 1/Bi = 100			Field Scale w 1/Bi = 0	
$V_{fracture}/V_{matrix}$	L_p	$E_{displacement}$	E_{tot}	$E_{displacement}$	E_{tot}
0.11	2.8	0.606	0.024	0.556	0.022
0.43	3	0.615	0.026	0.471	0.020
4	2.8	0.613	0.025	0.146	0.006

Here, penetration length, L_p doesn't change much when $V_{fracture}/V_{matrix}$ changes and thus isn't affected much by fracture to matrix volume. This implies that after primary production when the ratio of fracture to matrix ratio changes slightly due to the crushing of propped hydraulic fractures in the field, that change won't

significantly affect the penetration of a gas injection when EOR is performed. Since the fracture network shrinks with time and/or two-phase phenomena occurs during the production stage, evaluation of the fracture to matrix volume ratio in the field-scale requires a coupled geomechanical and flow modeling. Also, this shrinkage mainly affects soaking time significantly, and its effect on total recovery efficiency is almost negligible.

Total efficiency, however, is relatively constant for both lab and field scales and when both Biot numbers are applied. The relatively constant values of E_{tot} is proof that this model works in a systematic way. This is because, for varying values of fracture volume to matrix volume, the total efficiency values don't change much, as they are a function of the field factor. The sharp decrease in total efficiency for the field scale in the white column from 0.02 to 0.006 shows the pronounced effect which the Biot number has on the recovery efficiency. This aids in validating the systematic upscale prediction approach. Furthermore, from both Tables 5 and 6, the orange regions are well known from modeling and lab results. The white region, on the other hand, is only predicted, and can thus be verified with field data, where the field factor can be accurately determined.

Lab Scale	Field Scale
Diffusion	Diffusion, convection (dispersion)
1/Bi is often large	1/ Bi is very small
$V_{fracture}/V_{matrix}$ is large	$V_{fracture}/V_{matrix}$ is small

Figure 15. Sources of Discrepancies between Lab and Field-scale

From the table above, it can be seen that the choke effect is observed in the lab results and explained by modeling results. Hence, a slow production rate maximizes the recovery factor and should be considered in the field-scale.

4.2.2 Effect of Time on Recovery Factors

As part of the sensitivity analysis, injection time (T1) and soaking time (T2) were varied to find the effect of time on the recovery for the Huff-n-Puff process. This was run for different scenarios of Vf/Vm and D values. Production time was kept constant at 1 month. **Table 7** below displays the values for Vf/Vm of 0.11 at D = 1e-7 ft^2/s, **Table 8** presents values of Vf/Vm of 0.11 at D = 1e-8 ft^2/s, **Table 9** presents values of for Vf/Vm of 0.4 at D = 1e-7 ft^2/s and **Table 10** displays values of for Vf/Vm of 0.4 at D = 1e-8 ft^2/s.

Table 7. Table of varying injection and soaking times with constant production time, Vf/Vm = 0.11, D = 1e-7 ft^2/s.

Time (months)		Lab Scale		Field Scale	
T1	T2	E_{dis}	E_{tot}	E_{dis}	E_{tot}
0.25	0.25	0.28	0.01	0.31	0.012
0.25	0.5	0.36	0.014	0.4	0.015
0.25	1	0.48	0.018	0.53	0.02
0.5	0.25	0.37	0.014	0.41	0.015
0.5	0.5	0.44	0.016	0.48	0.018
0.5	1	0.54	0.02	0.58	0.022
1	0.25	0.47	0.017	0.51	0.019
1	0.5	0.51	0.019	0.56	0.021
1	1	0.59	0.022	0.64	0.024

As can be seen, the recovery factor is very sensitive to change in both injection and soaking times. The longer the injection and soaking period, the higher the recovery factor. This trend is seen even as the diffusion coefficient decreases from 10^-7 ft^2/s to 10 ^-8 ft^2/s as shown in **Table 8** below**.** Also, the field scale values are noticeably higher than the lab-scale values, where the Biot number accounts for all the unseen parameters in the model, as expected for a consistent Vf to Vmatrix value. However, when the Vf/Vm increases from 0.1 to 0.4, the recovery values go up for both the lab-scale and the field scale. This is because, since the fracture size is bigger than the matrix size, there is more space for the oil to flow into the matrix, and thus have a higher recovery.

Table 8. Table of Varying injection and soaking times with constant production time for Vf/Vm = 0.11 and D = 1e-8 ft^2/s.

Time (months)		Lab Scale		Field Scale	
T1	T2	E_{dis}	E_{tot}	E_{dis}	E_{tot}
0.25	0.25	0.31	0.009	0.31	0.01
0.25	0.5	0.38	0.013	0.42	0.013
0.25	1	0.5	0.017	0.55	0.019
0.5	0.25	0.39	0.012	0.43	0.013
0.5	0.5	0.47	0.013	0.5	0.018
0.5	1	0.55	0.015	0.59	0.02
1	0.25	0.49	0.016	0.53	0.016
1	0.5	0.55	0.015	0.59	0.013
1	1	0.62	0.02	0.67	0.024

Table 9. Table of Varying injection and soaking times with constant production time for Vf/Vm = 0.4 and D = 1e-7 ft^2/s

Time (months)		Lab Scale		Field Scale	
T1	T2	E_{dis}	E_{tot}	E_{dis}	E_{tot}
0.25	0.25	0.36	0.011	0.27	0.009
0.25	0.5	0.43	0.015	0.36	0.013
0.25	1	0.55	0.019	0.49	0.017
0.5	0.25	0.44	0.015	0.37	0.013
0.5	0.5	0.52	0.017	0.44	0.015
0.5	1	0.6	0.021	0.54	0.019
1	0.25	0.54	0.018	0.47	0.015
1	0.5	0.6	0.02	0.52	0.018
1	1	0.67	0.023	0.6	0.022

Table 10. Table of Varying injection and soaking times with constant production time for Vf/Vm = 0.4 and D = 1e-8 ft^2/s

Time (months)		Lab Scale		Field Scale	
T1	T2	E_{dis}	E_{tot}	E_{dis}	E_{tot}
0.25	0.25	0.31	0.01	0.32	0.02
0.25	0.5	0.41	0.015	0.41	0.014
0.25	1	0.52	0.018	0.55	0.02
0.5	0.25	0.39	0.013	0.46	0.015
0.5	0.5	0.48	0.019	0.52	0.019
0.5	1	0.55	0.018	0.62	0.023
1	0.25	0.53	0.022	0.64	0.017
1	0.5	0.53	0.022	0.6	0.016
1	1	0.63	0.025	0.68	0.025

4.2.3 Effect of Diffusion Coefficient

When the diffusion coefficient is varied, it has the most impact on the injection phase, but not so much the soaking and the production phase. As can be seen from **Figure 16** below, the slope of the curve increases as one moves from 10^-7 ft^2/s to 10^-10 ft^2/s

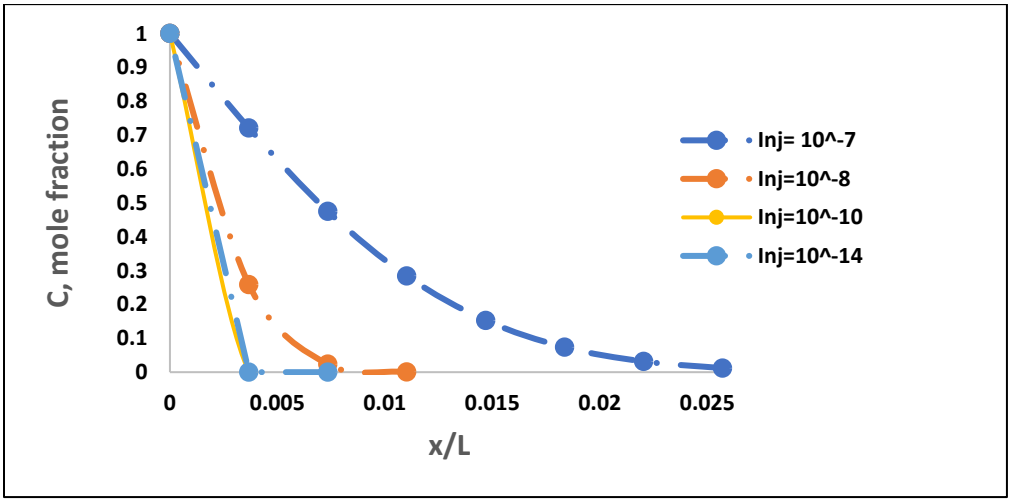

Figure 16. Effect of diffusion coefficient on Injection. Vfracture /Vmatrix = 0.11, L=70 m, T = 1 month

However, for soaking and production phases, this is not the case. A decrease from 10^-7 ft^2/s to 10^-8 ft^2/s sees a sharp increase in slope, as seen in Figure X below. This means that any injected gas remains in the fracture space and doesn't quite permeate into the matrix. There is some production from this system, however, it will obviously low, since the soaking phase doesn't contact more of the oil. Beyond 10^-8 however, it was impossible to determine the production profile, since it depends on the soaking profile, which goes to 1. Furthermore, it should be noted that for production, the model drops the diffusion coefficient even further by one order of magnitude, so recovery values are even much smaller. Also, this implies that, for formations with extremely low diffusion coefficients, more investigation is required for CO_2 EOR to be economical.

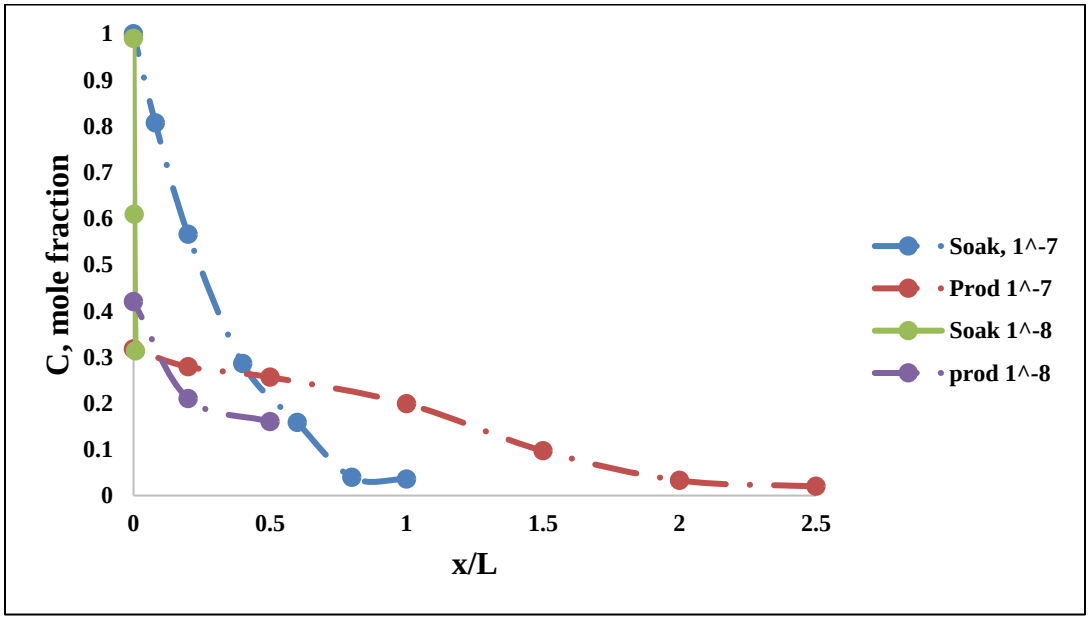

Figure 17. Effect of diffusion coefficient on soaking and production recovery. Vfracture /Vmatrix = 0.11, L=70 m, T = 1 month

These curves are corroborated by Zou, 2015, where the simulation used 4 different cases of diffusion computed using the Sigmund correlation with correction. Even though the diffusion coefficients vary in magnitude from the one used in this study as seen in **Table 11** and **Figure 18**, the same concept is proven in this case. The idea that diffusion plays a key role in CO2 huff-n-puff. The model used in this work serves to quantify how much that value is, based on the parameters discussed in this work.

Table 11. Diffusion coefficient values and the corresponding recovery factors.

Case 1	No Diffusion Coefficient	0
Case 2	Diffusion Coefficient X 0.1	3.43
Case 3	Diffusion Coefficient	10.59
Case 4	Diffusion Coefficient X 10	21.81

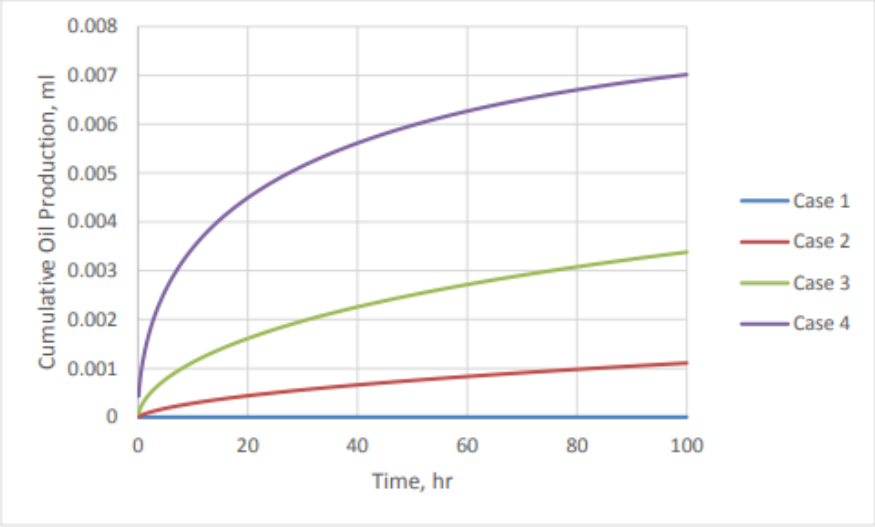

Figure 18. Cumulative oil production for cases with different diffusion coefficient values.

4.2.4 Effect of Fracture half-length on Recovery Factor

Figure 19 below shows the profile for a system with a fracture half-length of 100m. This is extremely similar to Figure 12 with a fracture half-length of 70 m. The recovery factor profile seems to be insensitive to the fracture half-length. This is because, after injection, the gas permeates the system only some penetration length, which is a tiny fraction of the actual length (penetration length is the length at which the system has 1% of concentration). Thus, when soaking takes place, it extends the Lp by only a little, and when production phase hits, the system's Lp at that point is the maximum Lp that will be achieved. Thus, L isn't much of a significant factor, but more so the time of the phases, and the diffusion coefficient of the systems.

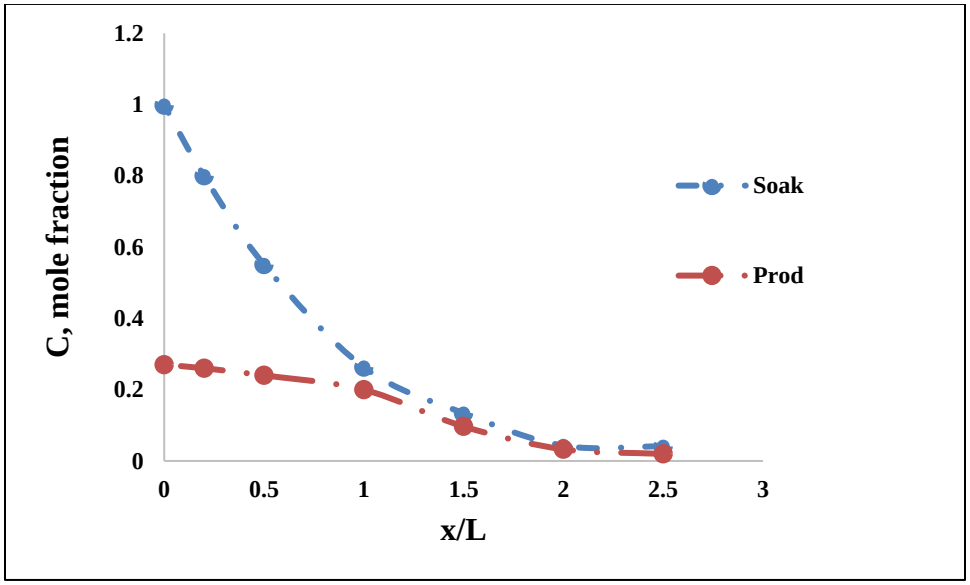

Figure 19. Effect of fracture half-length, L, on soaking and production recovery. Vfracture /Vmatrix = 0.11, D = 10^-7 ft^2/s, T = 1 month

Chapter 5 Field Factor Calculation

Most injection methods have been conducted in the Bakken, however, gas injection has been almost exclusively used in the Eagle Ford, making it ideal for this section analysis (Hoffman, 2018). This section attempts to validate the results of the field factor in the model proposed above. Two pilot projects in the Eagle Ford are used, as put forth in Hoffman, 2018. Throughout this chapter, they are referred to as Pilot B and Pilot C. This is to make it easy to reference in the Hoffman (2018) text by others. Three decline curves methods are used to determine the estimated ultimate recovery (EUR). Thereafter, the recovery factors are calculated, based on a determined original oil in place. These values are then used to back-calculate the field factors, as used in the model in previous chapters.

5.1 Geology

The Eagle Ford stretches across the Buda limestone under the Austin Chalk and is divided into two sections; an Upper and Lower sections (Workman and Grammer, 2013). As seen in **Figure 20**, this play spans much of southern Texas, with oil and gas windows from the Mexican border on the southwest to Gonzales and Lavaca counties to the northeast. The green dots represent the oil region, and the red dots represent the gas portion. Its reservoir matrix permeability is about 20 – 50 nD (Gibson, 2014), making it a tight play.

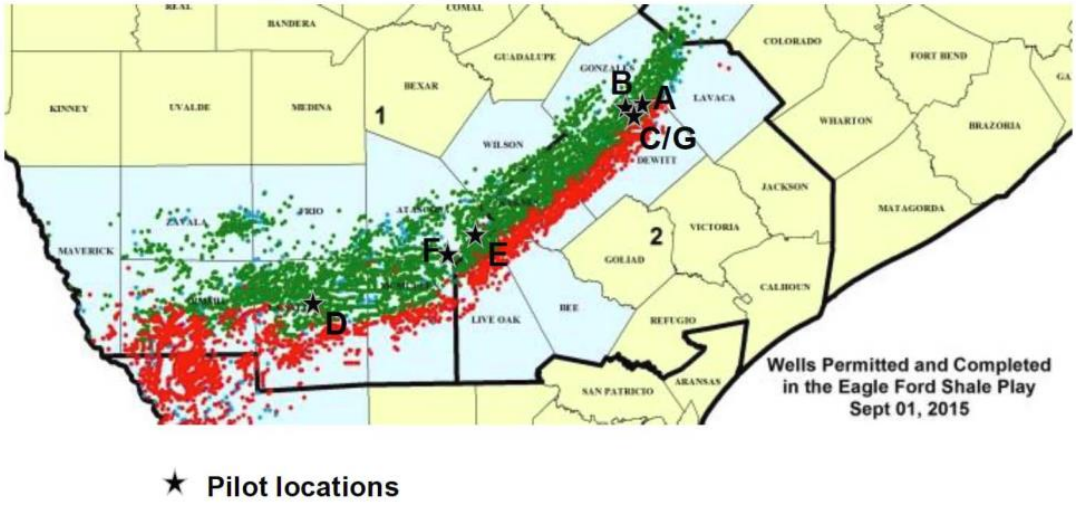

Figure 20 Location of pilot projects in the Eagle Ford wells and approximate locations of gas injection huff-n-puff pilots (Hoffman, 2018)

Table 12 General Information for Pilots

Pilot	Injection Year	County	# of wells in pilot	#wells in lease
B	2015	Gonzales	4	8
C	2015	Gonzales	6	14

Pilots B and C were chosen due to the similarities in their development. 4 injection and 4 non-injection wells are located in Pilot B. Whereas Pilot C 8 horizontal wells running from NW to SE, with others running perpendicular to these. More details for the pilots are provided in Hoffman, 2018. Pilot B was injected into for 1.5 years and produced for 2.5 years after that. Pilot C was injected into for 2.5 years and produced for 2.5 years after that. In order to determine the recovery factors, decline curve analysis is needed, and it is discussed below.

5.2 Decline Curve Analysis

Arps' (1945) decline curve is probably the most fundamental decline curve methods used throughout the decades for reserve estimation. Arps covers three different kinds of well behavior; exponential flow, harmonic flow and hyperbolic flow based on a b exponent value which will be discussed below.

The cumulative production is essentially the integral of the rate equation. That being said, it was developed for specifically for conventional reservoirs with boundary dominated flow regime. Thus, due to the low permeability and long-term transient flow combined with short production times, hydraulically fractured horizontal shale wells might not give accurate estimates (Gong, 2013). Due to multistage fracture treatments in shale, natural fractures resource depletion trend is fairly complex. Also, adsorbed gas contributes a significant fraction of total original gas in place (Tian et al., 2013) and its effect on EUR isn't well understood. Furthermore, Hui (2017) states the four common flow regimes in tight oil reservoirs including linear flow, bilinear flow, pseudo-radial flow in fractures and border-dominated flow. Also, that hydraulically fractured tight oil reservoirs have flows dominated by matrix-fracture linear flow (Hui, 2017). This flow regime is honored by the 3rd DCA ran for the production data.

The equations below were adopted from Khan and Callard, 2010, Kupchenko et al., 2008 and Fetkovich et al., 1996.

Arps Rate Time

$$q(t) = \frac{q_i}{(1+bD_i t)^{\frac{1}{b}}} \quad (17)$$

For b>0. For b = 0, the equation is reduced using calculus

$$q(t) = q_i e^{-D_i t} \quad (18)$$

The 2 above equations are used to determine rate.

Also to forecast reserves, cumulative production is calculated as the integral of the rate as follows:

$$N_p = \frac{q_i^b}{D_i(1-b)}\left[q_i^{1-b} - q^{1-b}\right] \quad (19)$$

This is used when b is not equal to 0. Using calculus the below equation is derived for when b = 1

$$N_p = \frac{q_i}{D_i}\log\left(\frac{q_i}{q}\right) \quad (20)$$

Now nominal decline is the instantaneous decline at a specific point in time, and is determined as follows:

$$D = \frac{D_i}{1+bD_i t} \quad (21)$$

$$EUR = N_{p_{data}} + Reserves \quad (22)$$

Where reserves is calculated from the Arps cumulative function above.

In the formulations above, q (t) is the flow rate, (bbl/day), qi = initial producing rate (bbl/day), D = nominal decline, Di = initial nominal decline rate, t = time, b is the decline constant (known as b exponent) – the larger it is, the longer the well produces and vice versa. Np is the cumulative oil produced, bbl, and EUR is the expected ultimate recovery, STB.

Rate Cumulative Analysis

Here, the original Arps cumulative production equations are rearranged to solve for rate, the following equations come out

$$q = \left[q_i^{1-b} - \frac{N_P D_i (1-b)}{q_i^b}\right]^{\frac{1}{1-b}} \quad (23)$$

This is used when b is not equal to 1. The equation below is used when b = 1

$$q = q_i e^{\frac{-N_p D_i}{q_i}} \quad (24)$$

In the formulations above, q (t) is the flow rate, (bbl/day), qi = initial producing rate (bbl/day), D = nominal decline, Di = initial nominal decline rate, t = time, b is the decline constant (known as b exponent) – the larger it is, the longer the well produces and vice versa. Np is the cumulative oil produced, bbl, and EUR is the expected ultimate recovery, STB.

Reciprocal Rate Cumulative Production

The following equation is used during the infinite acting region, during linear flow regime to calculate reciprocal rate. This is essentially derived from the Arps equation when b = 2 and solving for reciprocal rate

$$\frac{1}{q} = \frac{D_i}{q_i^2} N_p + \frac{1}{q_i} \quad (25)$$

$$D_i = \frac{m_{rrc}}{1/q_i^2} \quad (26)$$

$$t_{elf} = \frac{1}{q_i} N_p + \frac{1}{2} m_{rrc} N_p^2 \quad (27)$$

In the formulations above, q is the flow rate, (bbl/day), qi = initial producing rate (bbl/day), D = nominal decline, Di = initial nominal decline rate, t = time, b is the decline constant (known as b exponent) – the larger it is, the longer the well produces and vice versa. Np is the cumulative oil produced, bbl, m_rrc is the slope of the infinite acting linear flow plot, and t_elf is the time to the end of linear flow.

T_elf is shown in the plots by a red-bounded yellow triangle. This time is critical for forecasting. After the t_elf, the remaining data is fit with the Arps cumulative production.

Indras (2014) investigated hydraulically fractured wells in the Eagle Ford play and highlighted the linear flow regime experienced. Anderson and Matter discuss that linear flow regime is much more common and is virtually always observed in low permeability wells with hydraulic fractures, implying a negligible pressure drop in

the fractures, and that ultimate reserves for a well can be estimated with confidence only if BDF is reached (Anderson and Mattar 2003). In the two pilot cases presented here, boundary dominated flow is reached, and was used for determining EUR.

5.2.1 General Methodology for DCA

Production data up until start of injection is plotted on a rate-time, rate-cumulative and reciprocal rate-cumulative production plot. The appropriate equations above are used to calculate new data to be fit to the curve. A regression is done on the data, by minimizing the sum of the absolute relative error between predicted rates and actual rates, in order to get a close fit for the data. This is done by adjusting the qi, Di and b cells by using Excel's Solver.

Thereafter, the forecast is plotted on the same graph by taking the maximum time (last data point) and forecasting into the future to the economic limit. This rate takes into account qi, Di, b and the maximum time. Then, the instantaneous nominal decline at the last point is calculated from **eq. 21**. The reserves are then calculated based on **eq. 19** and **20**, using qi, Di at the end of production data. The EUR is then the sum of the cumulative production and the reserves.

Typically with an oil well, there is more noise in the data and it has to be cleaned. It also comes with a gas stream. However, in this analysis, the data presented from Hoffman (2018) is used directly. This serves as a means to validate the model's recovery factor/field factors calculated.

5.2.2 Decline Curve Analysis Results

For the DCA in Hoffman, 2018, a b-factor value of 1 (harmonic) is used. The DCA done in this section is fine-tuned to fit the data, giving a more accurate forecast prediction. If the well is shut for some time and it's later turned on full choke down the line, the entire fit is going to be inaccurate, and this will overestimate reserves. However, in this analysis, there is no information about shut-ins. That being said, a rate time plot is used as an initial DCA technique. Then, the rate-cumulative plot was used, followed by the reciprocal rate-cumulative plot as is discussed below.

In **Figure 21** below, a decline curve analysis is used on data for Pilot B. The blue line indicates the data before injection. This was initially plotted on the graph. Later, Arps' equation was used to fit a hyperbolic curve to this date, by minimizing the sum of squared errors. This was done by using an initial guess for b and Di, and later adjusting them to fit the curve. Thereafter, a forecast was done from the end of production into the future at the economic rate using the determined b, initial rate and nominal decline data from the initial fit. The economic limit for the Eagle Ford is determined from literature as 4 bbl (Wachtmeister et al., 2017). b values are reported in the Figure captions, and are less than the value of 1 used in Hoffman, 2018.

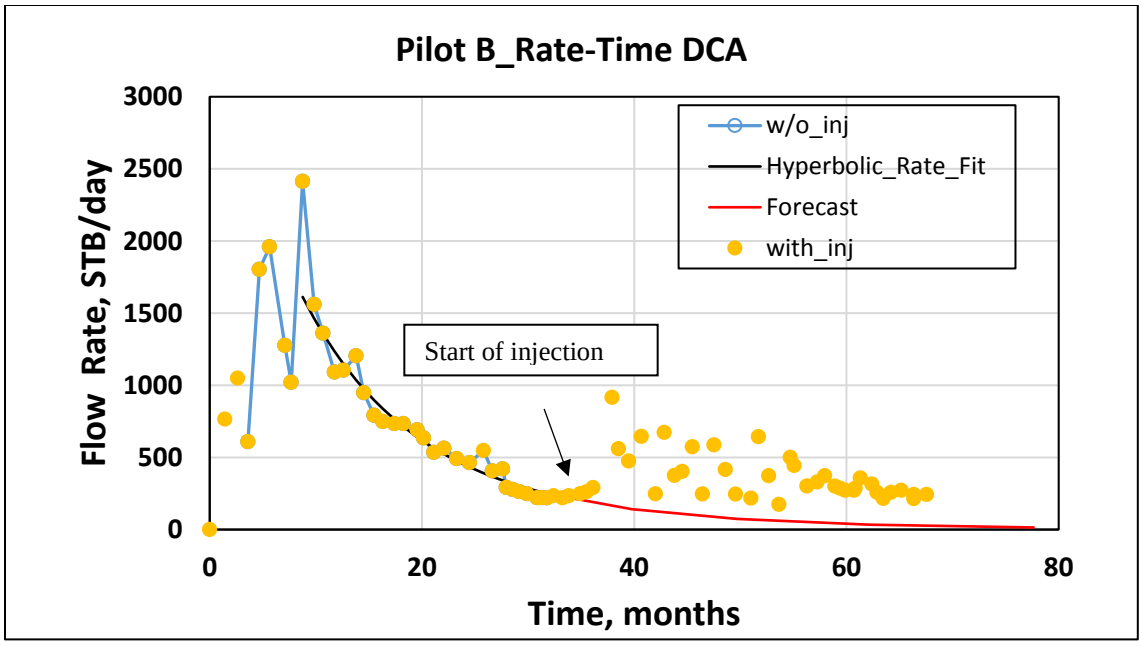

Figure 21 Pilot B Rate-Time DCA
b = 0.11, Di = 9%

A similar procedure was done for the rate-cumulative production plot as seen in **Figure 22**. Here, the rate cum plot is typically not affected by shut-ins, and is expected to give slightly better estimates. Even though it also neglects the flow regime changes and thus overestimates reserves, and it's relatively better than rate-time.

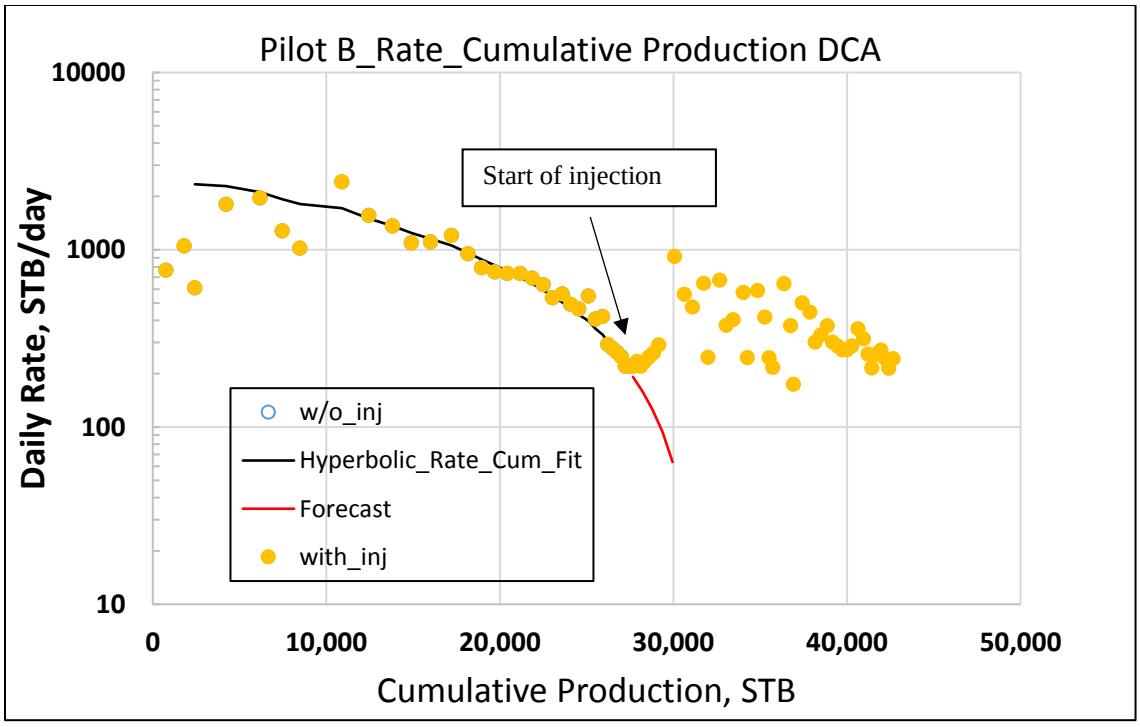

Figure 22 Pilot B Rate Cumulative Production DCA
b = 0.182, Di = 9.77%

Finally, to explore the presence of hydraulic fractures in the system, the reciprocal rate-cumulative function as seen in **Figure 23.** This method honors the linear flow regime often seen in hydraulically fractured wells. It is used for vertical wells and hydraulically fractured horizontal wells (Khan and Callard, 2010). The assumption here though is that the well is fractured and is exhibiting linear flow. From Hoffman (2018), the pilots used for the study are fractured wells, so this type of analysis fits better for forecasting. For this analysis, a plot of reciprocal rate vs linear production is made with the production data. The red line is used to fit the early time data which is used to simulate linear flow. For this analysis, an assumption of infinite acting

linear flow is made and constant bottom hole pressure during production is assumed.

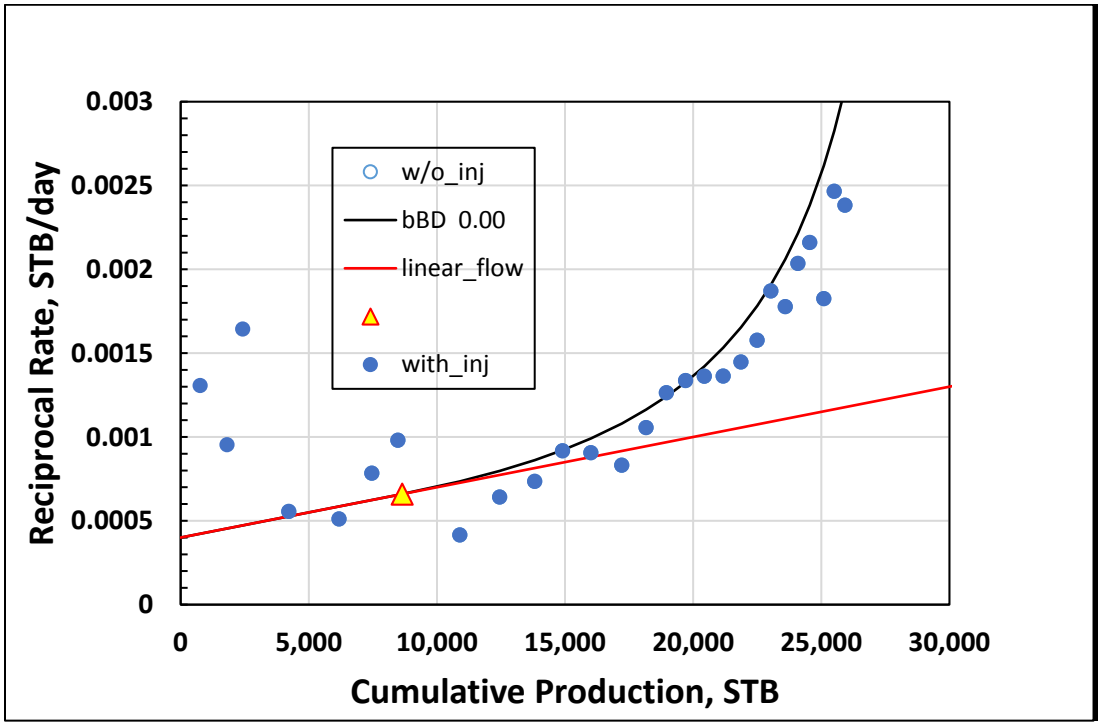

Figure 23 Pilot B Reciprocal Rate Linear Flow DCA
b_linear flow = 2, b_BD = 0.10, Di_BD = 6.4%

The above analysis is repeated for Pilot C, as seen in **Figures 24, 25** and **26**.

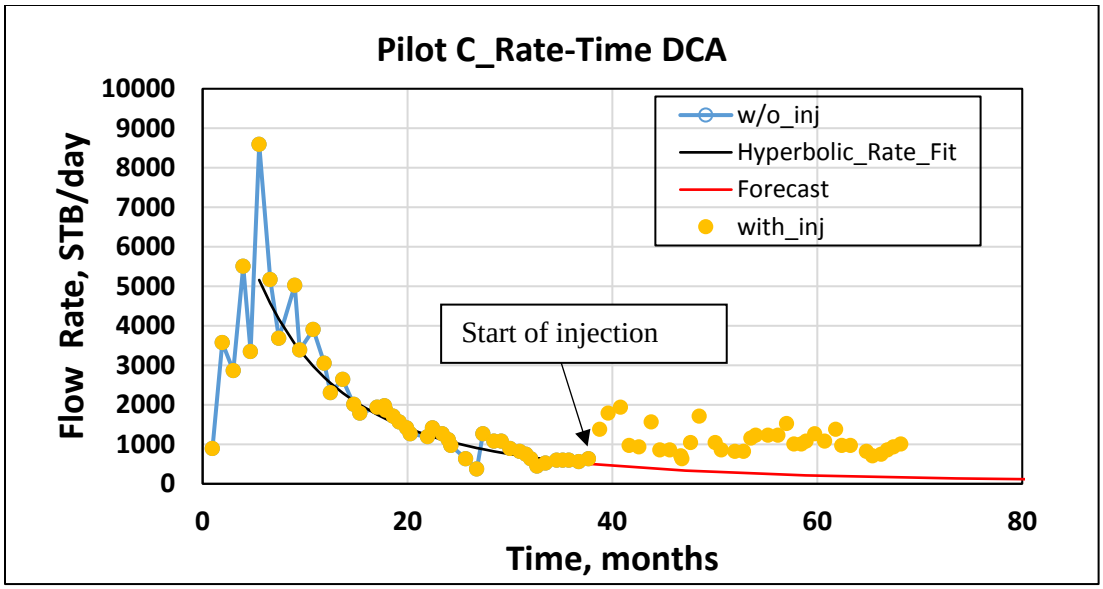

Figure 24 Pilot C Rate-Time DCA
b =0.380, Di = 11.6%

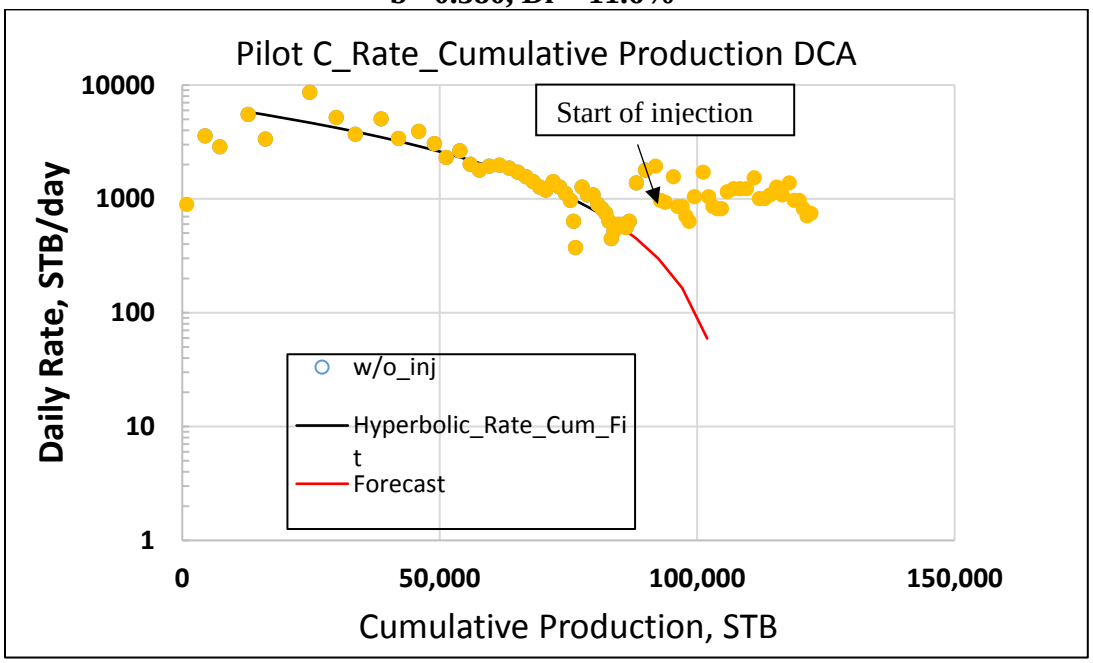

Figure 25 Pilot C Rate Cumulative Production DCA
b = 0.379, Di = 10.67%

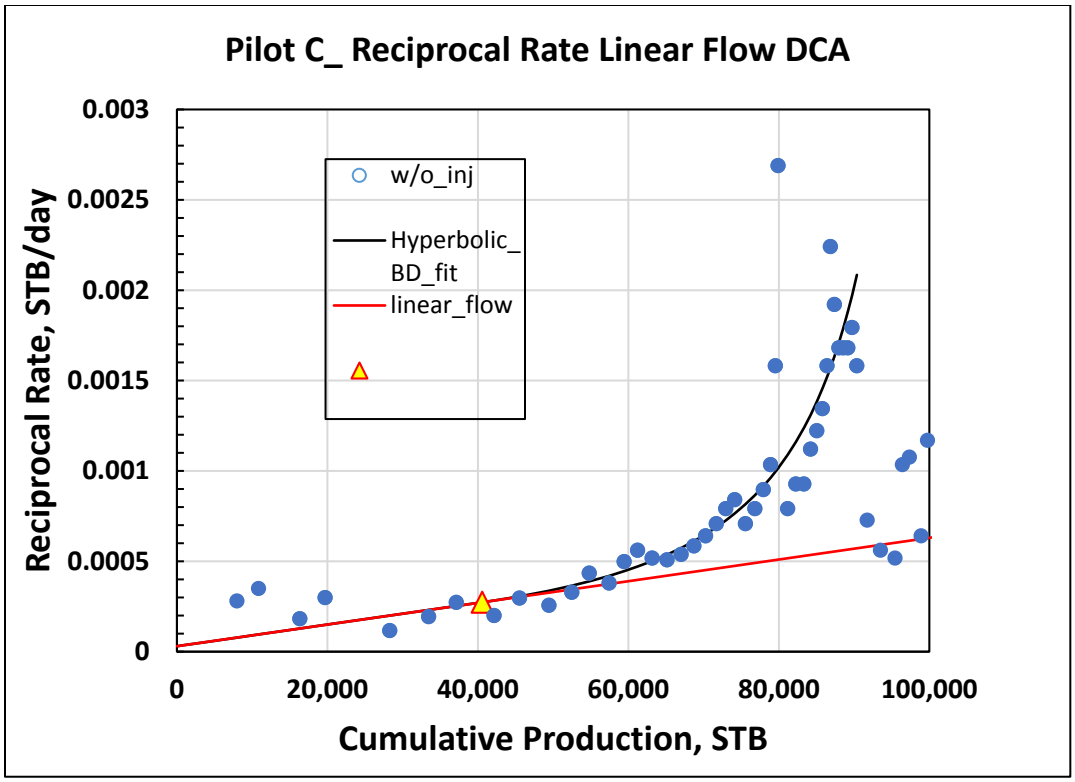

Figure 26. Pilot C Reciprocal Rate Linear Flow DCA,
b_linear flow = 2, b_BD = 0.310, Di_BD = 8%
BD = boundary dominated

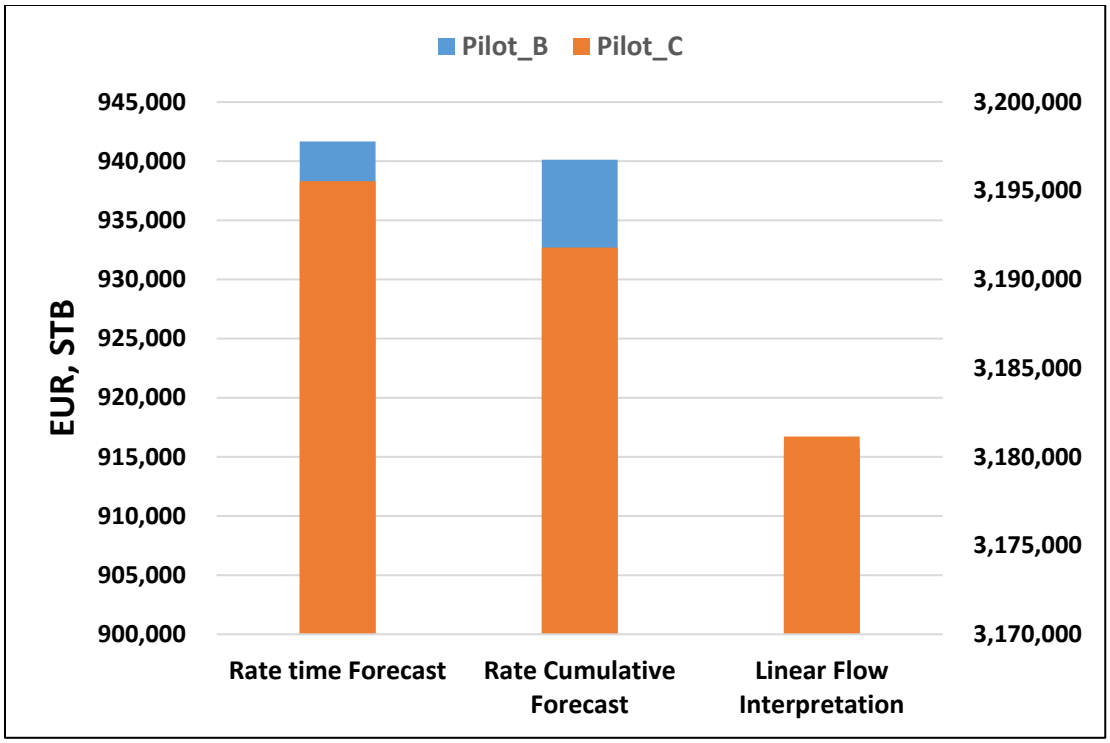

Figure 27 EUR Comparison of DCA methods

From Figure 27, it can be seen that the EUR values determined from the different methods are slightly different. The lowest is consistently the linear flow interpretation, which takes into account the hydraulic fractures in the system. This EUR value was thus used to determine the recovery factor, using 915,726 STB for Pilot B and 3,181,152 STB for Pilot C. With the results of the expected ultimate recovery, the original oil in place is determined as 30 MM STB, and used to calculate the recovery factor. Delaihdem (2013) ran various simulations with characteristic Eagle Ford shale reservoir properties and to analyze declines curves in that shale play. Thus, the calculations used for the original oil in place were taken

from these sources. Using a well spacing of 160 ft. (Lalehrokh, 2014) in these pilots, a drainage area of 640 acres is used to determine original oil in place.

$$N = \frac{7758\,Ah\phi(1-s_w)}{B_{oi}} \quad (28)$$

Where N = original oil in place, STB

A = drainage area, acres

h = reservoir thickness (130 ft., Delaihdem, 2013, Mullen, 2010)

S_w = water saturation (0.3, Delaihdem, 2013)

B_{oi} = formation volume factor (1.3 bbl/STB Delaihdem, 2013)

Original oil in place is calculated as 30 MM STB. Delaihdem's simulation results indicate 4.0% primary oil recovery factor and 5.8% enhanced shale oil recovery factor using CO_2 miscible injection (2013). These are close to ones determined for these pilots.

5.2.3 Determining the Field Factor

As can be seen in **Table 13** below, the cumulative oil production for Pilot C is significantly higher than that of Pilot B. This is because Pilot C has 6 wells, and one extra year of production. Also, Pilot B was injected for 1.5 years and produced for 1 year, while Pilot C was injected continuously for 2.5 years (Hoffman, 2018).

Table 13 Field factor calculation

	Pilot B (1.5 years_inj)	Pilot C (2.5 years_inj)
Np before injection, bbl	837,063.99	2,515,908.15
Np after injection, bbl	1,279,821.78	3,662,848.71
Np due to EOR, bbl	442,757.79	1,146,940.56
RF before injection	0.031	0.105
RP after injection	0.045	0.143
RF increase	0.015	0.038
Percent RF increase	0.484	0.366
Vf/Vm = 0.001, D = 10^{-10} ft^2/s		
RF_lab model	0.120	0.066
FF	0.125	0.576
Vf/Vm = 0.01 10^{-10} ft^2/s		
RF_lab model	0.124	0.118
FF	0.121	0.322
Vf/Vm = 0.1, D = 10^{-10} ft^2/s		
RF_lab model	0.159	0.180
FF	0.094	0.211

Where RF = recovery factor and FF = field factor and D = diffusion coefficient

The field factor here represents the additional recovery that will come from the EOR operation on the pilot. From eq. 2, field factor is calculated as

$$Field\ Factor = \frac{Recovery\ Factor_{\ pilot-scale}}{Recovery\ Factor_{\ lab-scale}} \quad (29)$$

The calculated field factor comes out between the range of 0 and 1 for varying fracture volume to matrix volume ratios. To get these values, the proposed model was run with an injection time of 1.5 years and 2.5 years for Pilot B, and injection time of 2.5 years and 2.5 years production for Pilot C. This resulted in a lab-scale

recovery factor value for Pilot B and Pilot C. When applied to the field scale recovery factors, the field factors were generated as seen above.

There is a variation in the field factor values calculated for both pilot projects. This could be explained by proppant embedment in the fracture system, or fracture closure due to long production of the wells.

Chapter 6 Conclusions

6.1 Main Contributions

The main contributions of the thesis are as follows:

1. Negligence of the accessibility factor, Biot number, and $V_{fracture}/V_{matrix}$ can explain the discrepancy between field-scale and lab-scale results.
2. The Biot number is an umbrella term for unknown field parameter conditions that influences field factor; it allows for the same equations to be successfully applied to both scales.
3. $V_{fracture}/V_{matrix}$ is a necessary parameter in EOR upscaling; it's mainly important during the soaking stage, and not very important for determining total field efficiency.
4. The choke effect in the cyclic gas injection is observed in the lab experiments and explained by modeling results. This phenomenon is significant on the lab scale. On the field scale, however, this choke effect happens mainly at the fracture-matrix interface. It also happens within the matrix itself and explained as a loss in connectivity. This is however taken care of by the Biot number. However, a slow production rate maximizes the recovery factor and should be considered in the pilot-scale. Therefore, there is a trade-off between how fast the oil is produced and how much ultimately

can be recovered and that the economic consideration will determine the optimal production rate.

5. The diffusion coefficient has the most impact on the injection phase, but not so much the soaking and production phase. Injected gas usually doesn't permeate the matrix for systems with low diffusion coefficients
6. The decrease in the diffusitivity coefficient decreases gas penetration length and decreases total displacement efficiency. Total displacement decreases because of the decrease in the accessibility factor
7. Vf/Vm influences recovery factor; from 0.1 to 0.4, the recovery values go up for both the lab-scale and the field scale
8. The recovery factor is very sensitive to change in both injection and soaking times. The longer the injection and soaking period, the higher the recovery factor.
9. Recovery factors are insensitive to the system's fracture half-length
10. Decline curve analysis is used to determine field factor values when values lie in the range of 0 and 1 for varying ratios of fracture volume to matrix volumes.

6.2 Limitations of the Outcome and Future Work

One of the model assumptions is that single phase is assumed. This may be the case during injection, but not so during production, and the author is aware of this. Production is usually in the two-phase regime. However, if two-phase is

considered, then capillary pressure has to be addressed, which is not in the scope of this work. More work should be done to include two-phase flow in order to have a more representative model.

Also, the diffusion coefficient used in this work is orders of magnitude larger than that used in some research work. For huff-n-puff, the system has micro fractures which extend from the regular fractures. Due to this, the distance of the front of CO_2 doesn't go a long way into the matrix because the micro fractured volume transmission is limited. So even though there are big fractures as seen in Figure 7, there are micro fractures also which limit the penetration length. Some simulation results have been published with natural fractures, however, this could be coupled with microseismic data to improve on this work, in terms of getting a better understanding of how stimulated reservoir volume affects huff-n-puff.

Furthermore, it should be noted that the diffusion coefficient is a mixture of diffusion and convection. Thus, to get the full picture, more modeling work has to be done to get a better understanding in order to improve the upscaling methodology.

Moreover, water interaction is not considered. More complex models could be built to account for this.

Nomenclature

A = drainage area, acres

A_c = contact area between the fracture network and the matrix, ft^2

b = choke effect

Bi = Biot number

B_{oi} = formation volume factor, bbl/STB

C = amount of free gas in the system, mol

C_0 = initial molar concentration, $mole/ft^3$

C_1 = final molar concentration, $mole/ft^3$

C_{inj} = amount of moles of gas injected into the system, mol/ft^3

C_{prod} = molar concentration per ft^3 of gas produced, $mole/ft^3$

C_{soak} = amount of moles of gas per ft3 infiltrating the system, $mole/ft^3$

C_μ = surface concentration of the adsorbed phase in kerogen, mol

$D_{pilot\text{-}scale}$ = diffusion rate at the field scale, ft^2/s

$D_{lab\text{-}scale}$ = diffusion rate, at the lab scale, ft^2/s

$L_{lab\text{-}scale}$ = half fracture spacing at the lab scale, ft

$L_{pilot\text{-}scale}$ = half fracture spacing at the field scale, ft

D = nominal decline, (DCA)

Di = initial nominal decline rate, (DCA), %

D_t = total diffusion rate within the matrix, ft^2/s

D_{matrix} = gas diffusion coefficient in the matrix, ft^2/s

D_f = Fickian diffusion, ft^2/s

D_{fr} = fractal dimension

D_k = Knudsen diffusion, ft^2/s

D_s = surface diffusivity of the adsorbed gas in the kerogen, ft^2/s

D_t = total diffusion rate, ft^2/s

DCA = Decline Curve Analysis

DDV = Dynamic Drainage Volume

DPV = Dynamic Penetration Volume

$E_{displacement}$ = Recovery displacement efficiency

E_{tot} = Total recovery efficiency

EOR = Enhanced Oil Recovery

EUR = Expected Ultimate Recovery

IIF = Injection Induced Fractures

IFT = Interfacial Tension

h = reservoir thickness, ft

$k_{fracture}$ = fracture permeability, mD

K = ratio of the volumes of matrix and fracture network

L = half fracture spacing, ft.

LSW = Low Salinity Water

L_p = distance of matrix penetrated by injected gas, ft.

m_rrc = slope of the infinite acting linear flow plot

N = original oil in place, STB

Np = cumulative oil produced, STB

q (t) = flow rate, bbl/day

qi = initial producing rate, bbl/day

SRV = Stimulated Reservoir Volume

S_w = water saturation, %

T = time, sec

t_elf = time to the end of linear flow, months

V_{matrix} = matrix volume

$V_{fracture}$ = fracture volume

X = dimensionless length

z = average pore coordination number

α = ratio of the volumes of fracture and matrix network

ω = weighting factor

ϕ = porosity, %

Γ = interconnectivity parameter

References

Adrian, D. Course materials for 10.37 Chemical and Biological Reaction Engineering, Spring 2007.

Anderson, David Mark, Louis Mattar. 2003. Material-Balance-Time During Linear and Radial Flow. Proc., Canadian International Petroleum Conference, Calgary, Alberta.

Hassan Ali, Hassan Soleimani, Noorhana Yahya, Leila Khodapanah, Maziyar Sabet, Birol M.R. Demiral, Tanvir Hussain, Lawal Lanre Adebayo. 2020. Enhanced oil recovery by using electromagnetic-assisted nanofluids: A review, Journal of Molecular Liquids, Volume 309.

Arps, J.J. 1945. Analysis of Decline Curves. AIME 160: 228-247.

Alfarge, D., Wei, M., Bai, B., 2017. IOR Methods in Unconventional Reservoirs of North America: Comprehensive Review. Iraqi Ministry of Oil; Missouri University of Science and Technology. SPE– 185640-MS

Alharthy, N., Teklu, T., Kazemi, H., Graves, R. 2015. Enhanced Oil Recovery in Liquid Rich Shale Reservoirs: Laboratory to Field. *Society of Petroleum Engineers*. DOI:10.2118/175034-MS

Alvarez, J. O., Neog, A., Jais, A., & Schechter, D. S. (2014). Impact of Surfactants for Wettability Alteration in Stimulation Fluids and the Potential for Surfactant EOR in Unconventional Liquid Reservoirs. *Society of Petroleum Engineers*.doi:10.2118/169001 MS SPE-180270-MS15

Alvarez, J.O. and Schechter, D.S. 2015. Wettability Alteration and Spontaneous Imbibition in Unconventional Liquid Reservoirs by Surfactant Additives. *Society of Petroleum Engineers*. DOI: 10.2118/177057MS.

Chen, C. Ballhoff, M.T., & Mohanty, K., K. (2014). Effect of Reservoir Heterogeneity on Primary Recovery and CO2 Huff-n-Puff Recovery in Shale-Oil Reservoirs. Society of Petroleum Engineers.

Clark, A. J., (2009). Determination of Recovery Factor in the Bakken Formation, Mountrail County, ND. *Society of Petroleum Engineers*. STU.

Crank, J. 1975. The Mathematics of Diffusion, Brunel University, Uxbridge. SecondEdition.

Dang, Son. 2019. Understanding the Fundamental Drive Mechanisms for Huff-n Puff Enhanced Oil Recovery in Tight Formations. PhD Dissertation. University ofOklahoma, Norman, Oklahoma.

Darugar, Q., Heinisch, D., Lundy, B. J., Witte, P., Wu, W., & Zhou, S. (2016, November 7). Estimating Ultimate Recovery and Economic Analysis of Shale Oil Wells in Eagle Ford and Bakken. Society of Petroleum Engineers.

Davudov, D., Moghanloo, R. G., Dadmohammadi, Y., Curtis, M., & Javadpour, F. (2016a, June). Impact of Pore Topology on Gas Diffusion and Productivity in Barnett and Haynesville Shale Plays. In ASME 2016 35th International Conference on Ocean, Offshore and Arctic Engineering (pp. V008T11A032 V008T11A032). American Society of Mechanical Engineers.

Davudov, D., Moghanloo, R. G., & Yuan, B. (2016b, August). Impact of Pore Connectivity and Topology on Gas Productivity in Barnett and Haynesville Shale Plays. In Unconventional Resources Technology Conference, San Antonio, Texas, 1-3 August 2016 (pp. 2790-2806). Society of Exploration Geophysicists, American Association of Petroleum Geologists, Society of Petroleum Engineers.

Davudov, D., & Moghanloo, R. G. (2016, September 26). Upscaling of Pore Connectivity Results from Lab-Scale to Well-Scale for Barnett and Haynesville Shale Plays. Society of Petroleum Engineers.

Davudov, D., & Moghanloo, R. G. (2018). Impact of pore compressibility and connectivity loss on shale permeability. International Journal of Coal Geology.

Dawson, M., Nguyen, D., Champion, N., & Li, H. (2015). Designing an Optimized Surfactant Flood in the Bakken. *Society of Petroleum Engineers*. doi:10.2118/175937-MS

Delaihdem, Dieudonne K. 2013. Decline curve analysis and enhanced shale oil recovery based on Eagle Ford Shale data. Master's Thesis. University of Alaska. Alaska, USA

EIA. 2016. https://www.eia.gov/analysis/studies/drilling/pdf/upstream.pdf

Fetkovich, M. J., Fetkovich, E. J., & Fetkovich, M. D. (1996, February 1). Useful Concepts for Decline Curve Forecasting, Reserve Estimation, and Analysis. Society of Petroleum Engineers. doi:10.2118/28628-PA

Gibson, A. T. 2014. Paleoenvironmental Analysis and Reservoir Characterization of the Late Cretaceous Eagleford Formation In Frio County, Texas, USA. Master's Thesis. Colorado School of Mines.

Gong, X. 2013. Assenssment of Eagleford Shale Oil and Gas Resources. PhD thesis. Texas A&M University, Texas, USA.

Hawthorne, S. B., Gorecki, C. D., Sorensen, J. A., Steadman, E. N., Harju, J. A., Melzer, S., 2013. Hydrocarbon mobilization mechanisms from Upper, Middle, and Lower Bakken reservoir rocks exposed to CO2. *SPE Unconventional Resources Conference Canada*

Hoffman, B. T., and Evans J., (2016). Improved Oil Recovery IOR Pilot Projects in the Bakken Formation. SPE-180270- MS paper presented at the SPE Low Perm Symposium held in Denver, Colorado, USA, 5–6 May 2016.

Hoffman, B. T. (2018, March 13). Huff-N-Puff Gas Injection Pilot Projects in the Eagle Ford. Society of Petroleum Engineers. doi:10.2118/189816-MS

Hoteit, H. and Firoozabadi, A. 2006. Numerical Modeling of Diffusion in Fractured Media for Gas Injection and Recycling Schemes. Presented at the SPE AnnualTechnical Conference and Exhibition, San Antonio, Texas, USA, 24–27 September. SPE-103292-MS. http://dx.doi.org/10.2118/103292 MS.

Hui, P., Qiquan, R., Yong, L., & Min, T. (2017, June 1). Performance Analysis and Flow Regime Identification of Fractured Horizontal Wells in Tight Oil Reservoirs. Society of Petroleum Engineers. doi:10.2118/188071-MS

Hu, Q., Ewing, R. P., & Dultz, S. (2012). Low pore connectivity in natural rock. *Journal of contaminant hydrology*, *133*, 76-83.

Indras, Purvi. Applying Decline Curve Analysis in the Liquid-Rich Shales: Eagleford Shale Study. Master's Thesis. Texas A&M Univeristy, College Station, Texas

Jacobs, T., 2016, EOR-For-Shale: Ideas to boost output gain traction, JPT, June, 28-31.

Jiang, Z., Zhang, W., Liang, C., Wang, Y., Liu, H., and Chen, X. 2016. Basic characteristics and evaluation of shale oil reservoirs, Petroleum Research, Volume 1, Issue 2, Pages 149-163,

Kaiser, M. J., & Yu, Y. (2010). Economic limit of field production in Texas. Applied Energy, 87, 3235–3254.

Khan, M. U., & Callard, J. G. (2010, January 1). Reservoir Management in Unconventional Reservoirs. Society of Petroleum Engineers. Paper SPE 130146 presented at the SPE Hydrocarbon Economics and Evaluation Symposium Dallas, Texas. USA 8-9 March, 2010.

Kovscek, A.R., Tang, G.-Q., and Vega, B. 2008. Experimental Investigation of Oil Recovery from Siliceous Shale by CO2 Injection. Presented at the SPE Annual Technical Conference and Exhibition, Denver, 21–24 September. SPE-115679 MS. http://dx.doi.org/10.2118/115679-MS

Kupchenko, C. L., Gault, B. W., & Mattar, L. (2008, January 1). Tight Gas Production Performance Using Decline Curves. Society of Petroleum Engineers.

Lake, W. L. 1989. *Enhanced Oil Recovery*. Englewood Cliffs, New Jersey. Prentice Hall

Lalehrokh, F., & Bouma, J. (2014, September 30). Well Spacing Optimization in Eagle Ford. Society of Petroleum Engineers. doi:10.2118/171640-MS

LeFever, J., & Helms, L., 2008, Bakken Formation Reserve Estimates, North Dakota Geological Survey.

Mikhailov, M., D., Ozisik, M., N. 1984. Unified Analysis and Solutions of Heat and Mass Diffusion. Technical University, Bulgaria, North Carolina State University, North Carolina. Dover Edition.

Moghanloo, R. G., Javadpour, F. and Davudov, D. 2013. Contribution of methane molecular diffusion in kerogen to gas-in-place and production. SPE paper presented at Western Regional & AAPG Pacific Section Meeting, Monterey, CA, USA.

Moghanloo, R. G. and Hosseinipour, S.S. 2014. Mechanistic Modeling of Fluid Flow in Shale" URTEC Paper 1921547 presented at the SPE/AAPG/SEG Unconventional Resources Technology Conference, 25-27 August Denver, Colorado, USA.

Mozafari M, Nasri Z (2017) Operational conditions effects on Iranian heavy oil upgrading using microwave irradiation. J Pet Sci Eng 151:40–48

Moghanloo, R. G. and Lake, L.W.2012. Applying Fractional Flow Theory under Loss ofMiscibility. SPEJ 17(3): 661-6770.

Mullen, J., 2010, Petrophysical Characterization of the Eagle Ford Shale in South Texas: Society of Petroleum Engineers, SPE Canadian Unconventional Resources and International Petroleum Conference in Calgary, CSUG/SPE 138145.

Pu, H., and Li, Y., (2016). Novel Capillarity Quantification Method in IOR Process in Bakken Shale Oil Reservoirs. SPE-179533-MS presentated at the SPE Improved Oil Recovery Conference held in Tulsa, Oklahoma, USA, 11–13 April 2016

Shafiai, S.H., Gohari, A. Conventional and electrical EOR review: the development trend of ultrasonic application in EOR. J Petrol Explor Prod Technol (2020).

Sheng, J. J., and Chen K., 2014. Evaluation of the EOR potential of gas and water injection in shale oil reservoirs. *Journal of Unconventional Oil Gas Resources* 5, 1–9

Sheng, J. J., 2015. Enhanced oil recovery in shale reservoirs by gas injection. *Journal of Natural Gas Science & Engineering* 22, 252–259

Song, C., & Yang, D. (2013). Performance Evaluation of CO2 Huff-n-Puff Processes in Tight Oil Formations. *Society of Petroleum Engineers*. doi:10.2118/167217-MS.

Sorensen, J. A. and Hamling. J.A. 2016. Enhanced oil recovery: historical Bakken test data provide critical insights on EOR in tight oil plays. *The American Oil and Gas Reporter*

Sun, J., Zou, A., and Schechter, D., 2016. Experimental and numerical studies of CO2 EOR in unconventional liquid reservoirs with complex fracture networks. *SPE IOR Conference*

Tian, Yao & Ayers, Walter & McCain, William. (2013). The Eagle Ford Shale Play South Texas: Regional Variations in Fluid Types Hydrocarbon Production and Reservoir Properties. 10.2523/IPTC-16808-MS.

Tinni, A., Sondergeld, C., and Rai, C., 2017. Pore connectivity between different wettability systems in organic-rich shales. *Society of Petroleum Engineers*. doi:10.2118/185948- PA

Tong Shen, Rouzbeh Ghanbarnezhad Moghanloo, and Wei Tian. 2017. Decoupling of Channeling and Dispersion Effects by Use of Multiwell Tracer Test. SPE Reservoir Evaluation & Engineering. In Press. DOI. https://doi.org/10.2118/187960-PA

Tovar, F. D., Eide, O., Graue, A., and Schechter, D. S., 2014. Experimental investigation of enhanced recovery in unconventional liquid reservoirs using CO2: a look ahead to the future of unconventional EOR. *SPE Unconventional Resources Conference*

USGS, 2013. Petroleum resource assessment of the Bakken and Three Forks formation.

Vega, B., O'Brien, W.J., and Kovscek, A.R. 2010. Experimental Investigation of Oil Recovery from Siliceous Shale by Miscible CO2 Injection. Presented at the SPE Annual Technical Conference and Exhibition, Florence Italy, 19–22 September. SPE-135627-MS.

Wachtmeister, H., Lund, L., Aleklett, K., Hook, M. Production Decline Curves of Tight Oil Wells in Eagle Ford Shale. Nat Resour Res 26, 365–377 (2017).

Wan, T., Sheng, J. J., & Soliman, M. Y. (2013). Evaluate EOR Potential in Fractured Shale Oil Reservoirs by Cyclic Gas Injection. *Society of Petroleum Engineers*. doi:10.1190/URTEC2013-187

Wan, T. and Sheng, J.J. 2015. Evaluation of the EOR potential in hydraulically fractured shale oil reservoirs by cyclic gas injection, Petroleum Science and Technology, 33:7, 812-818.

Wan T., 2015. Investigation of EOR performance in shale oil reservoirs by cyclic gas injection. *Doctoral dissertation*. Texas Tech University

Wan, T., & Sheng, J. (2015). Compositional Modeling of the Diffusion Effect on EOR Process in Fractured Shale- Oil Reservoirs by Gas flooding. *Society of Petroleum Engineers*. doi:10.2118/2014-1891403-PA.

Wang, D., Butler, R., Liu, H., & Ahmed, S. (2011, August 1). Flow-Rate Behavior and Imbibition in Shale. Society of Petroleum Engineers. doi:10.2118/138521-PA

Wang, D., Butler, R., Zhang, J., & Seright, R. (2012, December 1). Wettability Survey in Bakken Shale With Surfactant-Formulation Imbibition. Society of Petroleum Engineers. doi:10.2118/153853-PA

Wang, D., Zhang, J., Butler, R., and Olatunji, K., (2016). Scaling Laboratory-Data Surfactant Imbibition Rates to the Field in Fractured-Shale Formations. *Society of Petroleum Engineers*. http://dx.doi.org/10.2118/178489-PA.

Wang, Lei & Tian, Ye & Yu, Xiangyu & Wang, Cong & Yao, Bowen & Wang, Shihao & Winterfeld, Philip & Wang, Xu & Yang, Zhenzhou & Wang, Yonghong & Cui, Jingyuan & Wu, Yu-Shu. (2017). Advances in improved/enhanced oil recovery technologies for tight and shale reservoirs. Fuel.

Wang, Zhenjun & Fang, Ri & Guo, Hangyuan. (2019). Advances in ultrasonic production units for enhanced oil recovery in China. Ultrasonics Sonochemistry. 60. 104791. 10.1016/j.ultsonch.2019.104791.

Workman, S. J., & Grammer, G. M. (2013). Integrating depositional facies and sequence stratigraphy in characterizing unconventional reservoirs in the Cretaceous (Cenomanian Turonian) Eagle Ford Shale, South Texas. Gulf Coast Association of Geological Societies Transactions, v. 63, p. 473 508.

Wu, K., Li, X., Guo, C., Wang, C., & Chen, Z. (2016, October 1). A Unified Model for Gas Transfer in Nanopores of Shale-Gas Reservoirs: Coupling Pore

Diffusion and Surface Diffusion. Society of Petroleum Engineers. doi:10.2118/2014-1921039 PA

Yuan, B., Zheng, D. Moghanloo, R. G., Wang, K. 2017. A Novel Integrated Workflow for Evaluation, Optimization, and Production Predication in Shale Plays. International Journal of Coal Geology. **180** (1):18-28.

Yu, Y., and Sheng, J. J. 2015. An Experimental Investigation of the Effect of Pressure Depletion Rate on Oil Recovery from Shale Cores by Cyclic N2 Injection. Unconventional Resources Technology Conference. doi:10.15530/URTEC 2015 2144010

Yu, W., Zhang, Y., Varavei, A., Sepehrnoori, K., and Zhang, T., 2018. Compositional simulation of CO_2 huff-n-puff in Eagle Ford tight oil reservoirs with CO_2 molecular diffusion, nanopore confinement and complex natural fractures. *SPE IOR Conference*

Zhu, P., Balhoff, M. T., & Mohanty, K. K. (2015). Simulation of Fracture-to Fracture Gas Injection in an Oil-Rich Shale. *Society of Petroleum Engineers*. doi:10.2118/175131 MSSPE-180270-MS17

Zhang, K 2016. Experimental and Numerical Investigation of Oil Recovery from Bakken Formation by Miscible CO2 Injection SPE Paper 184486 presented at Annual Technical Conference and Exhibition, 26-28

Zou, A. F. 2015. Thesis on Compositional Simulation of CO2 Enhanced Oil Recovery in Unconventional Liquid Reservoirs. Texas A&M University, Texas, USA.